EXPLORING THE PROPERTIES OF A COMBINED DIFFERENTIAL-MODE EQUALIZER AND COMMON-MODE FILTER

BY

COLIN THOMAS MADIGAN

THESIS

Submitted in partial fulfillment of the requirements
for the degree of Master of Science in Electrical and Computer Engineering
in the Graduate College of the
University of Illinois at Urbana-Champaign, 2015

Urbana, Illinois

Adviser:

Professor José E. Schutt-Ainé

ABSTRACT

As differential signaling becomes more and more desirable, innovative solutions must be sought to keep size and cost to a minimum. This thesis analyzes a combination differential-mode equalizer and common-mode filter (DME-CMF) realized on a two-layer microstrip board. Measurements up to 25 GHz are taken to explore the functionality of this device at and above the design frequency. The basics of S-parameters are reviewed, and the concept is expanded to include differential networks. Results in the form of differential S-parameters and eye diagrams are analyzed to judge the effectiveness of the DME-CMF, and future signal integrity applications are discussed.

Do, or do not. There is no try.

ACKNOWLEDGMENTS

This thesis could not have been completed without the support of many individuals. I would like to thank my fellow members of the Signal Integrity research group, especially Drew Handler and Xu Chen, for providing help where needed, and support every step along the way. I thank Tom Comberiate for getting me interested to join the research group in the first place, and for excellent instruction during my first semester. I owe special thanks to Professor José Schutt-Ainé for advising me throughout my graduate studies, and for helping to provide direction for this thesis. Finally, I must thank my parents, Nancy and Tom, for their love and support of my every endeavor for the past 24 years and counting.

TABLE OF CONTENTS

CHAPTER 1

INTRODUCTION

1.1 Motivation

In recent years, the technology of high-speed interconnects has been rapidly evolving. As data rates become faster, signal integrity concerns become increasingly more problematic. Higher data rates lead to more intersymbol interference (ISI), and differential signaling – common in high-speed channel design – can add noise through unwanted mode conversion. In general, after transmission along a lossy channel, differential-mode signals require equalization to combat the resulting ISI. Likewise, in order to recover the desired signal when common-mode noise is present, the noise must be suppressed with filtering. Both noise and ISI must be effectively mitigated to ensure the functionality of the interconnect.

Recently, a common solution for both problems was proposed: a passive device that acts as both a differential-mode equalizer and a common-mode filter, realized on a two-sided microstrip printed circuit board (PCB) [1]. This solution, also referred to as the DME-CMF, was designed with the aim of minimizing cost, size, and power consumption, while operating reliably at data rates of up to 8 Gb/s. The purpose of this thesis is to help the reader understand the DME-CMF and the concepts used to characterize its operation, to show that the results of [1] are reproducible, and to explore higher-frequency applications through microwave measurements and signal integrity analysis.

1.2 Outline

Because it is not inherently clear how the DME-CMF achieves its dual functionality, some analysis of the equivalent circuit models of the microstrip structures is necessary. Chapter 2 establishes the theory behind the DME-CMF. To verify the operation of a high-frequency device, a common method is to measure its scattering parameters. Chapter 3 reviews the derivation of scattering parameters, and expands the definition to include differential applications. In chapter 4, the process of fabricating and measuring new DME-CMF PCBs is discussed, and the results are shown and analyzed. Finally, chapter 5 summarizes this thesis and provides thoughts for future work with this technology.

CHAPTER 2

THE DME-CMF

At first, combining an equalizer and a filter into one device might seem counterintuitive; equalizers exist to increase signals, while filters are designed to remove them. But because the signals targeted to be increased and removed (the data being sent differentially and the common-mode noise, respectively) are measured in different ways, this task becomes feasible with the right structure.

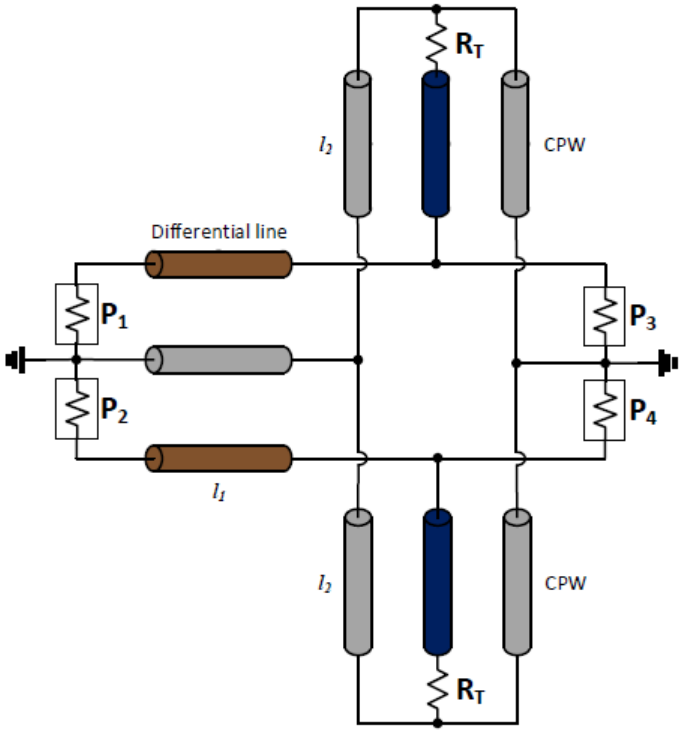

Figure 2.1: The equivalent circuit model for the DME-CMF, adapted from [1]

Figure 2.1 presents the equivalent circuit model for the DME-CMF. Line l_1 represents a differential coupled line, equivalent to a channel for differential

data transmission. This line pair has characteristic impedances Z_{even}^{Diff} and Z_{odd}^{Diff}, for the even- and odd-modes, respectively. The outer (brown) lines are the signal lines, while the middle (gray) line is the ground line. These lines are most easily implemented using a microstrip or stripline design. The vertical coupled lines with length l_2 represent coplanar waveguides (CPWs), with even- and odd-mode impedances of Z_{even}^{CPW} and Z_{odd}^{CPW}, respectively. The center (blue) lines are the signal lines, while the outer (gray) lines are ground. The CPW lines are terminated to ground with resistance R_T. The CPW structure is the part most responsible for the functionality of the DMC-CMF, and is implemented using a defected ground structure (DGS) [2].

2.1 Equalization

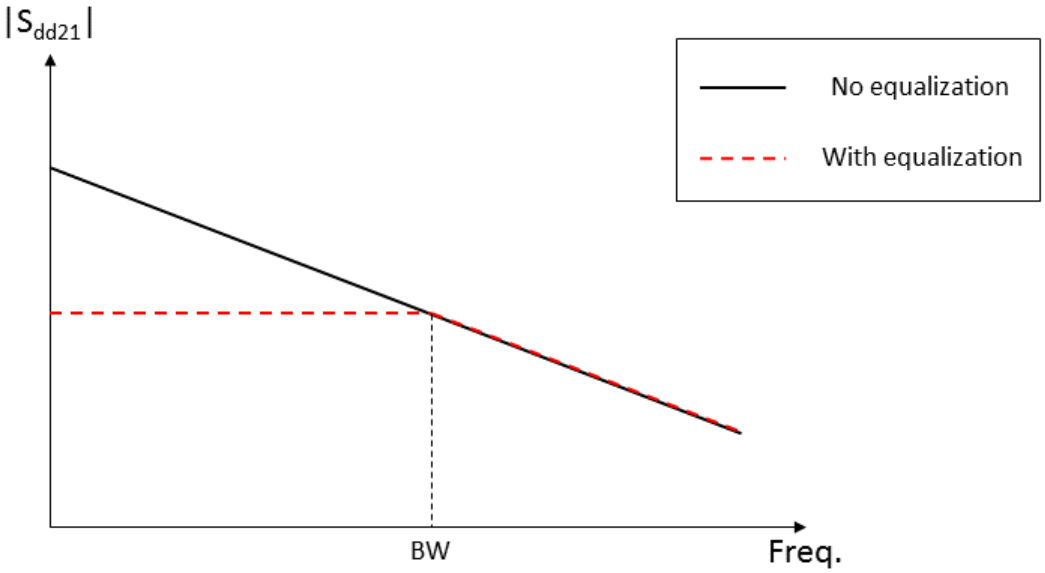

Figure 2.2: An example of equalization with a passive equalizer

With a passive equalizer, the goal is to flatten the magnitude of the differential insertion loss, $|S_{dd21}|$, as seen in Figure 2.2. This helps to negate frequency-dependent interconnect loss by bringing the magnitude of S_{dd21} for all frequencies within the bandwidth to a common level. Analysis in [1] shows the equalizer imposing a high-pass effect on differential-mode signals up to about 6 GHz.

2.2 Filtering

The common-mode noise filtering properties of the DME-CMF stem from two sources: the impedance discontinuity between the lines l_1 and l_2 in Figure 2.1, and the absorption due to R_T. Other types of common-mode filters include ferrite chokes or LTCC-based filters [3], but DGS-type filters are most popular for small, low-cost applications. Frequency-domain measurements in [1] confirm effective filtering, with common-mode noise down to -9.4 dB at DC, and a minimum at 7.4 GHz.

CHAPTER 3

DIFFERENTIAL SYSTEM CHARACTERIZATION

To analyze any device, we must be able to fully characterize the interactions between all inputs and outputs. For linear, time-invariant devices operating in the RF and microwave regimes, the most common method is to define the scattering parameters, or S-parameters, of the device. However, for a differential system, with two ports making up every input and output, we care only about the effects these combined differential ports have on each other. Therefore, we must modify the standard S-parameter definition for differential applications.

3.1 Scattering Parameters

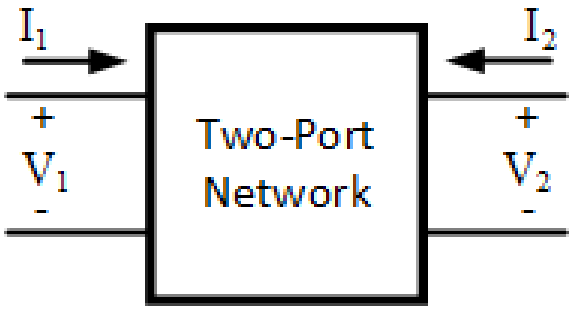

Figure 3.1: A two-port network

Perhaps the most intuitive way to define a network is by examining the relationships of the voltages and currents at every port. Figure 3.1 depicts a simple two-port network. From this, we can define an impedance, or **Z**, matrix such that

$$\begin{bmatrix} V_1 \\ V_2 \end{bmatrix} = \begin{bmatrix} Z_{11} & Z_{12} \\ Z_{21} & Z_{22} \end{bmatrix} \begin{bmatrix} I_1 \\ I_2 \end{bmatrix} \tag{3.1}$$

This is essentially a network-level application of Ohm's law. Each term Z_{ji} is calculated by finding the voltage-to-current ratio given by

$$Z_{ji} = \left.\frac{V_j}{I_i}\right|_{I_x=0\,\forall\, x\neq i}$$

So all ports except for port i are left open, which implies that $I_i = 0$ for every port except for port i. Therefore, calculating each Z_{ji} becomes simple. Networks can also be defined in terms of admittances such that $\mathbf{I} = \mathbf{YV}$, where $\mathbf{Y} = \mathbf{Z}^{-1}$ is the admittance matrix, and individual admittances Y_{ji} are found by shorting all ports except port i. These parameters are intuitive, and fully define any network. However, issues arise when we start dealing with devices at higher frequencies. When operating in the RF and microwave regimes, it becomes very difficult to terminate devices with shorts or opens without negatively affecting the performance, so we cannot measure Z or Y parameters. Instead, we can terminate ports with a reference impedance equal to the characteristic impedance of the network, usually 50 Ω, and measure the S-parameters. Instead of relating currents and voltages, S-parameters relate incident and reflected power waves on each port to fully characterize the system. We define these power waves such that

$$a_i = \frac{V_i + Z_0 I_i}{2\sqrt{Z_0}} \tag{3.2a}$$

$$b_i = \frac{V_i - Z_0 I_i}{2\sqrt{Z_0}} \tag{3.2b}$$

From this point forward, the power waves defined in (3.2) can be used to replace the example two-port in Figure 3.1 with the equivalent two-port in Figure 3.2. From these equations, we define the S-parameters for any network as

$$S_{ji} = \left.\frac{b_j}{a_i}\right|_{a_x=0\,\forall\, x\neq i} \tag{3.3}$$

For a two-port network, we can relate the incident and reflected waves using the S-parameters such that

$$\begin{bmatrix} b_1 \\ b_2 \end{bmatrix} = \begin{bmatrix} S_{11} & S_{12} \\ S_{21} & S_{22} \end{bmatrix} \begin{bmatrix} a_1 \\ a_2 \end{bmatrix} \tag{3.4}$$

So, for example, S_{21} is the reflected wave at port 2 due to an incident wave at port 1.

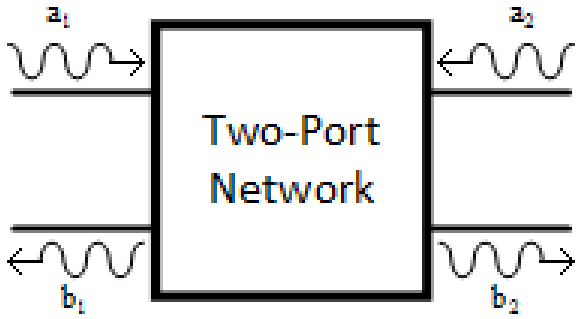

Figure 3.2: A two-port network with power waves

3.1.1 Some Properties of S-parameters

Again, S-parameters are a complete description of a network. This is useful for protecting intellectual property, as the functionality of a device can be modeled and simulated using its S-parameters without divulging the exact make-up of the device. This is called "black box" modeling. Other useful metrics can be extracted from S-parameters. From S_{21}, we can extract the insertion loss of a device, or the loss added to a system due to the insertion of a device into the system. This is defined as

$$\text{Insertion Loss} = -20\log_{10}|S_{21}| \text{ (dB)} \tag{3.5}$$

Likewise, S_{11} gives us the input return loss, which we will simply call the return loss. Essentially, this gives us information on how well the input impedance of the network is matched to the network impedance, Z_0. It is calculated by

$$\text{Return Loss} = -20\log_{10}|S_{11}| \text{ (dB)} \tag{3.6}$$

Another important property of S-parameters is that for passive networks, they are reciprocal. Reciprocity is such that if a two-port is constructed using only passive circuit elements, then the scattering matrix $\mathbf{S}$ will be symmetric, i.e. $S_{12} = S_{21}$ [4].

Note that, while the examples presented thus far are for two-port networks, S-parameter theory holds and is completely viable in defining systems with any number of ports. For an n-port system, elements of $\mathbf{S}$ are still calculated using (3.3), and the ports are related such that

$$\begin{bmatrix} b_1 \\ b_2 \\ \vdots \\ b_n \end{bmatrix} = \begin{bmatrix} S_{11} & S_{12} & \cdots & S_{1n} \\ S_{21} & S_{22} & \cdots & S_{2n} \\ \vdots & \vdots & \ddots & \vdots \\ S_{n1} & S_{n2} & \cdots & S_{nn} \end{bmatrix} \begin{bmatrix} a_1 \\ a_2 \\ \vdots \\ a_n \end{bmatrix} \tag{3.7}$$

3.2 Mixed-Mode S-parameters

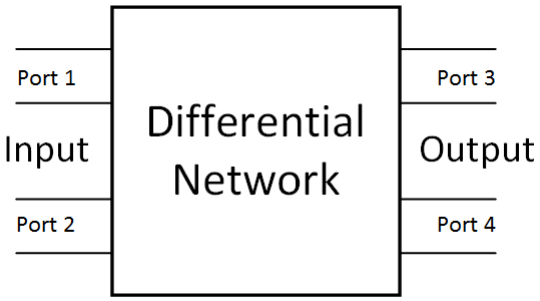

(a) A differential device represented as a four-port network

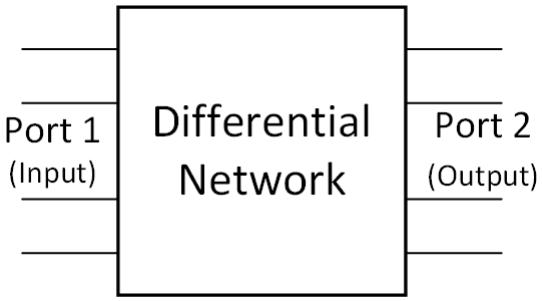

(b) A differential device represented as a two-port network

Figure 3.3: Multiple representations of a differential network

Now that S-parameters have been defined and their use justified, we can see that they should be a good way to characterize the DME-CMF circuit. However, one issue remains: it is not clear how to define the S-parameters of a differential network. In the case of the DME-CMF, we can see rather easily that, based on our current understanding of S-parameters for single-ended

circuits, we would classify it as a four-port network. However, we also know that the ports on one side of the circuit make up a differential input pair, while the ports on the other side are a differential output pair. We want each port to represent a single input or output, and thinking differentially, it would make sense for each pair to be represented by a single port. Figure 3.3 illustrates the difference between these two approaches.

It turns out that S-parameters can be modified to represent differential devices. If we have the single-ended S-parameters of a four-port network such as Figure 3.3a, we can calculate what are called the mixed-mode S-parameters of a two-port differential system such as Figure 3.3b. "Mixed-mode" refers to the two types of signal transmission in differential systems: differential mode (DM) and common-mode (CM). The mixed-mode S-parameters give us information about both modes. To derive these parameters, we need to first define the general properties of a differential system. For a differential port n comprising single-ended ports a and b, we say that

$$V_{dn} = V_a - V_b \tag{3.8a}$$

$$I_{dn} = \frac{I_a - I_b}{2} \tag{3.8b}$$

$$V_{cn} = \frac{V_a + V_b}{2} \tag{3.8c}$$

$$I_{cn} = I_a + I_b \tag{3.8d}$$

where V_d and I_d are the DM voltages and currents, and V_c and I_c are the CM voltages and currents. Additionally,

$$Z_d = 2Z_{oo} \tag{3.9a}$$

$$Z_c = \frac{Z_{oe}}{2} \tag{3.9b}$$

where Z_{oo} and Z_{oe} are the odd- and even-mode impedances, respectively. We can now define DM and CM power waves, a_{dn}, b_{dn}, a_{cn} and b_{cn}, which are related to $V_{(d,c)n}$, $I_{(d,c)n}$ and $Z_{(d,c)}$ in the same manner that (3.2) relates V_i, I_i and Z_0 to calculate a_i and b_i.

3.2.1 S-parameter Conversion for a Differential Two-Port

For a differential two-port system, we can use (3.8), (3.9) and the resulting power wave definitions to present an easy-to-use conversion from single-ended to mixed-mode S-parameters [5]. We can relate the DM and CM reflected power waves $b_{(d,c)n}$ to the incident power waves $a_{(d,c)n}$ with a matrix $\mathbf{S}$ such that

$$\begin{bmatrix} b_{d1} \\ b_{d2} \\ b_{c1} \\ b_{c2} \end{bmatrix} = \begin{bmatrix} \begin{bmatrix} S_{dd11} & S_{dd12} \\ S_{dd21} & S_{dd22} \end{bmatrix} & \begin{bmatrix} S_{dc11} & S_{dc12} \\ S_{dc21} & S_{dc22} \end{bmatrix} \\ \begin{bmatrix} S_{cd11} & S_{cd12} \\ S_{cd21} & S_{cd22} \end{bmatrix} & \begin{bmatrix} S_{cc11} & S_{cc12} \\ S_{cc21} & S_{cc22} \end{bmatrix} \end{bmatrix} \begin{bmatrix} a_{d1} \\ a_{d2} \\ a_{c1} \\ a_{c2} \end{bmatrix} \tag{3.10}$$

where

$$S_{ghij} = S_{(\text{output-mode})(\text{input-mode})(\text{output-port})(\text{input-port})}$$

In (3.10), S_{dd} are the DM S-parameters, S_{cc} are CM S-parameters, and S_{dc} and S_{cd} are mode conversions that occur from measuring the CM response when excited by a DM signal, and vice versa. These extra mode conversions are unavoidable, but generally not used for meaningful analysis. Now we can relate these mixed-mode power waves to the single-ended waves. For a mixed-mode power wave α representing either incident (a) or reflected (b) waves,

$$\alpha_{d1} = \frac{\alpha_1 - \alpha_2}{\sqrt{2}} \tag{3.11a}$$

$$\alpha_{c1} = \frac{\alpha_1 + \alpha_2}{\sqrt{2}} \tag{3.11b}$$

$$\alpha_{d2} = \frac{\alpha_3 - \alpha_4}{\sqrt{2}} \tag{3.11c}$$

$$\alpha_{c2} = \frac{\alpha_3 + \alpha_4}{\sqrt{2}} \tag{3.11d}$$

This gives us a direct conversion between single-ended and differential power waves. Expressing (3.11) in matrix form, we have

$$\mathbf{a}^{mm} = \mathbf{M}\mathbf{a}^{se} \tag{3.12a}$$

$$\mathbf{b}^{mm} = \mathbf{M}\mathbf{b}^{se} \tag{3.12b}$$

where $\mathbf{a}^{mm}$ and $\mathbf{b}^{mm}$ represent mixed-mode waves, $\mathbf{a}^{se}$ and $\mathbf{b}^{se}$ represent single-ended waves, and

$$\mathbf{M} = \frac{1}{\sqrt{2}} \begin{bmatrix} 1 & -1 & 0 & 0 \\ 0 & 0 & 1 & -1 \\ 1 & 1 & 0 & 0 \\ 0 & 0 & 1 & 1 \end{bmatrix} \tag{3.13}$$

We can use this matrix to convert directly from single-ended to mixed-mode S-parameters, such that

$$\mathbf{S}^{mm} = \mathbf{M}\mathbf{S}^{se}\mathbf{M}^{-1} \tag{3.14}$$

where $\mathbf{S}^{se}$ are the single-ended four-port S-parameters and $\mathbf{S}^{mm}$ are the mixed-mode S-parameters from (3.10). Note that this will only work if the four ports are numbered in the same manner as shown in Figure 3.3a.

3.3 Signal Integrity

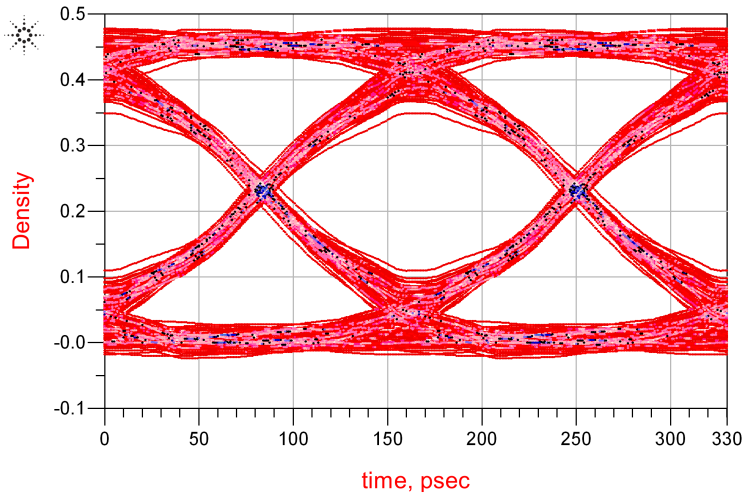

Figure 3.4: An eye diagram

While S-parameters are very useful in characterizing a system in the frequency domain, we also need a way to verify functionality in the time domain. One of the best figures of merit for this is the eye diagram. As seen in Figure 3.4, an eye diagram is a visualization of signal quality as it relates

to distortion, such as intersymbol interference and noise. We can make both qualitative and quantitative determinations about a signal by examining the features of the eye. In general, the larger the eye opening, the less distorted the signal. The shrinking, or "closing" of the eye signifies increased distortion of the signal [6].

Another common issue in signal integrity is that of dispersion. Dispersion is the frequency-dependence of the propagation constant of a medium [7]. One manifestation of dispersion is in the phase of S-parameters. Ideally, the phase of some example S_{21} should cycle linearly and periodically from $+180°$ to $-180°$. When dispersion is present, the phase will appear nonlinear. Practically, this can result in data arriving at the output of a channel at unexpected times. Additionally, as frequency increases on a line, higher order modes can propagate on the line, causing large amounts of dispersion that are very hard to combat.

CHAPTER 4

MEASUREMENTS AND RESULTS

4.1 Board Design and Fabrication

In order to verify functionality of the CME-DMF circuit and assess the potential for new applications through measurements, copies of the boards must first be manufactured. Three boards were designed and built: a small board containing only the DME-CMF (Board SD, Figures 4.1 and 4.2), a board with the DME-CMF following a long differential channel (Board LD, Figure 4.3), and a reference board with only a long channel and no DME-CMF (Board REF, not shown). The boards were designed using CadSoft EAGLE PCB Design, and manufactured in-house at the University of Illinois. Table 4.1 contains the physical parameters of board SD, which are labeled on Figure 4.4. All DME-CMF parameters are the same on board LD, with the only difference being the channel length, which is 800 mm. All the boards were made using 0.06" thick FR-4 laminate, with 1 oz. copper on both sides. Additionally, the resistors used were 0603 SMD packages.

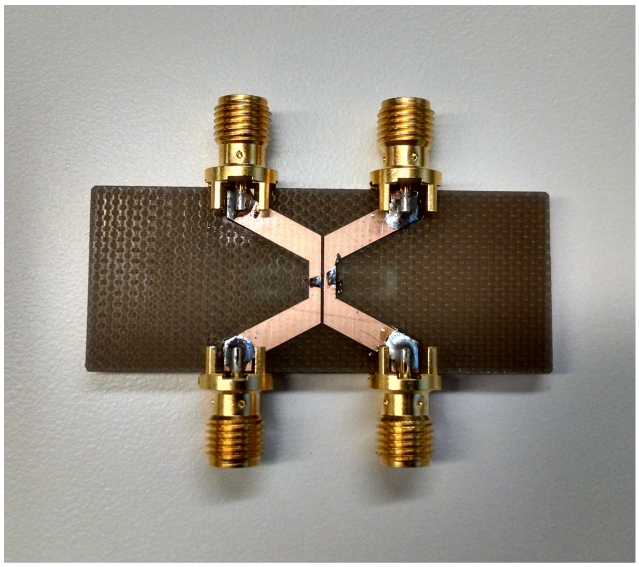

Figure 4.1: Board containing only the DME-CMF

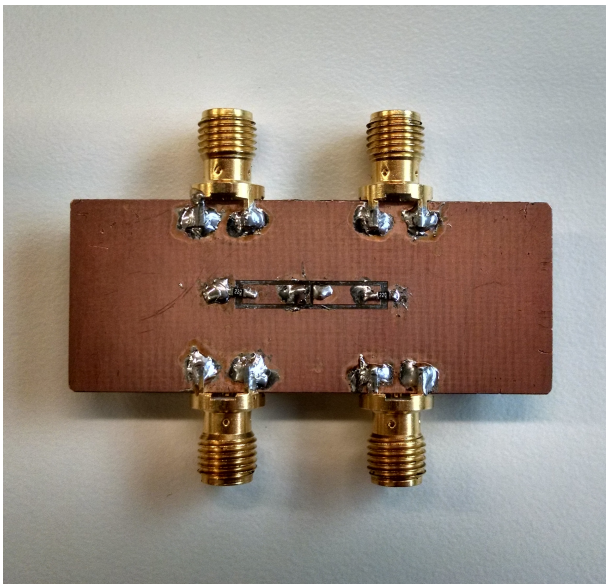

Figure 4.2: Back side of the DME-CMF containing the CPW equalizer

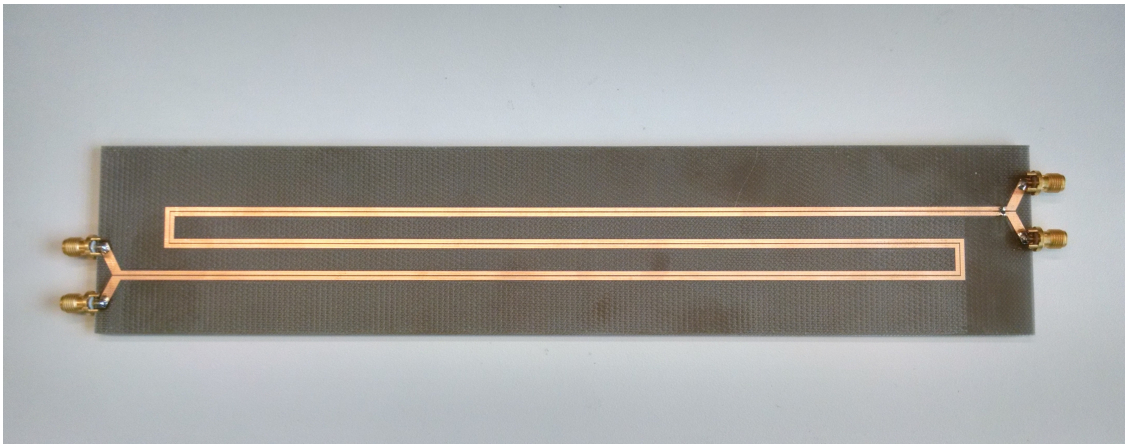

Figure 4.3: Board containing the DME-CMF at the end of a long channel

Table 4.1: Parameter Values

Parameter	Value
W_g	50 mm
l_1	20 mm
W_d	0.85 mm
S_d	0.32 mm
W_0	2 mm
W_s	2 mm
l_s	7 mm
g	0.5 mm
R_T	22 Ω

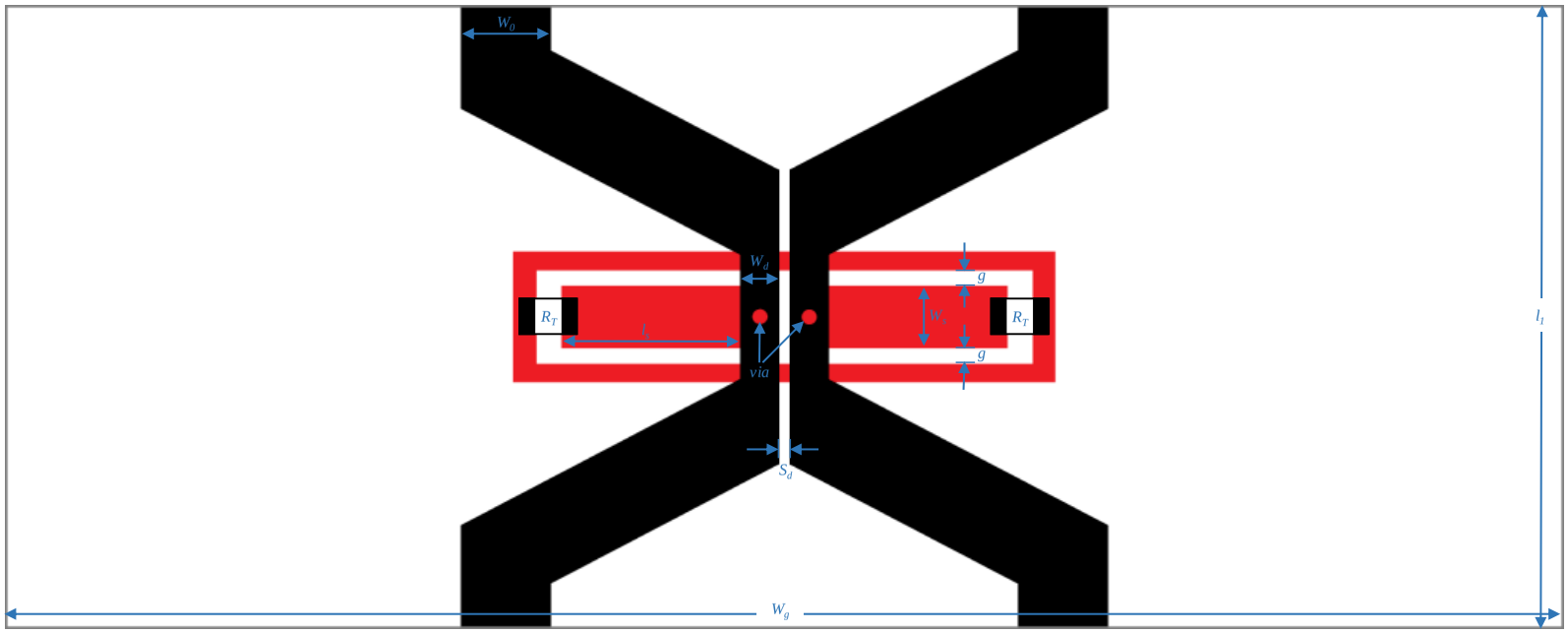

Figure 4.4: Visualization of the DME-CMF with dimensions

4.2 Measurement Procedures

The goal was to fully characterize the boards over a frequency range larger than the original designated range of operation. As such, all three boards were measured with two separate sweeps: first, from 300 kHz to 9 GHz using an Agilent E8358A PNA Series network analyzer, with 801 frequency points, and second, using an HP 8510C network analyzer, from 9 GHz to 25 GHz, again with 801 points. The reason for splitting the sweeps is because the E8358A can measure a lower range of frequencies than the 8510C.

Before measuring, calibration was performed on the system using the Agilent 85052D SOLT calibration kit. Detailed information on calibration techniques can be found in [8]. Since both network analyzers used are two-port devices, and the boards to be measured have four ports, multiple measurements must be made for each board to ensure complete characterization. For each frequency range of interest, six two-port measurements were taken per board. It is important that, for each two-port measurement, the two disconnected ports be terminated by 50Ω loads as seen in Figure 4.5.

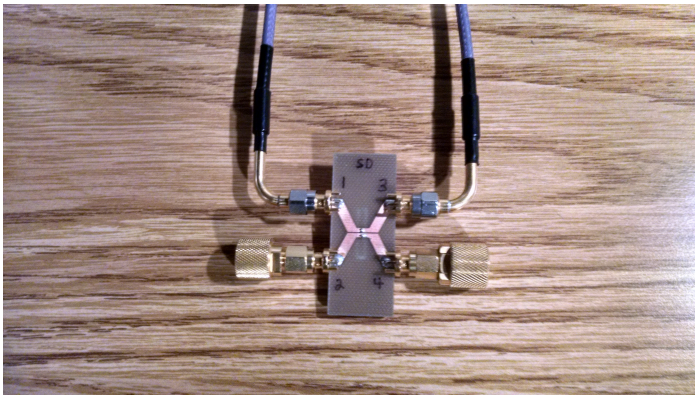

Figure 4.5: Setup for each two-port measurement between ports 1 and 3, with ports 2 and 4 terminated by 50Ω loads.

The six two-port Touchstone files can be combined into a single four-port file using the ADS Touchstone Combiner, as seen in Figure 4.6. After the .s4p file is generated, it can be converted into mixed-mode S-parameters using the methodology outlined in section 3.2. The MATLAB code used to carry out the conversion can be found in Appendix A. The resulting S-parameters are presented in section 4.3.

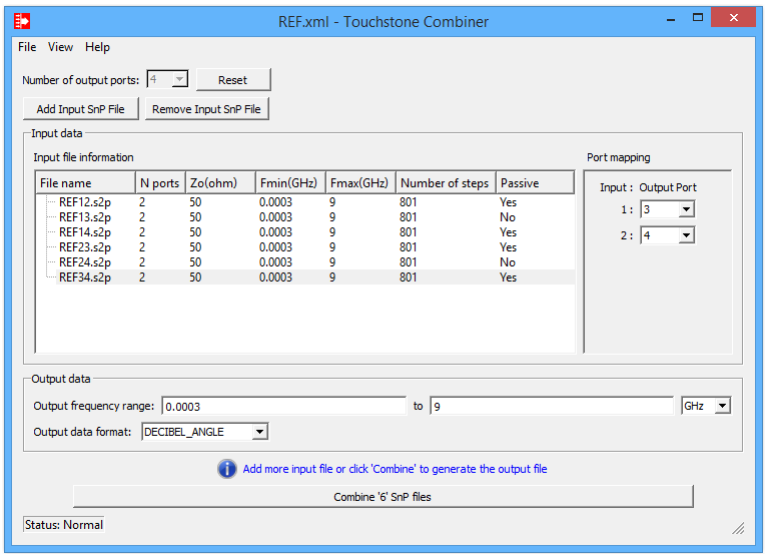

Figure 4.6: Touchstone Combiner, used to convert multiple .s2p files into a single .s4p file.

4.3 Results

To evaluate the three boards that were measured, we can look at the data in a few different ways in order to learn more about their functionality. Subsection 4.3.1 presents magnitude plots of, followed by observations about, the DM and CM S-parameters, both as a point of comparison to the work done in [1] and to explore higher-frequency behavior. Subsection 4.3.2 presents plots of, followed by observations about, the DM and CM phase response, to check for dispersion. Finally, subsection 4.3.3 presents eye diagram simulations at multiple data rates to judge the quality of equalization as the operating frequency changes.

4.3.1 Magnitude Response

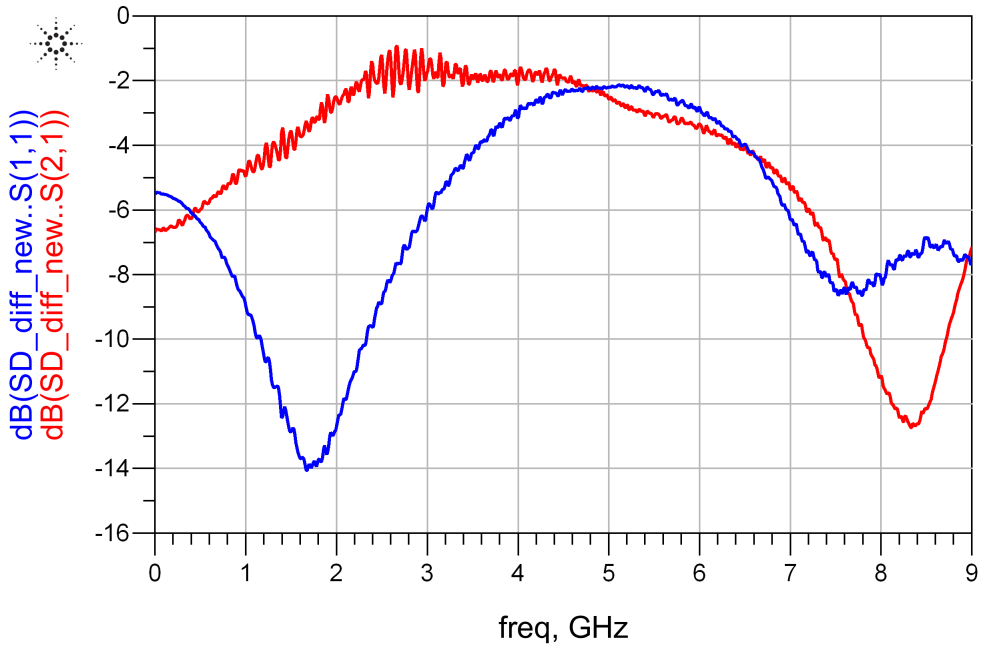

(a) 300 kHz to 9 GHz

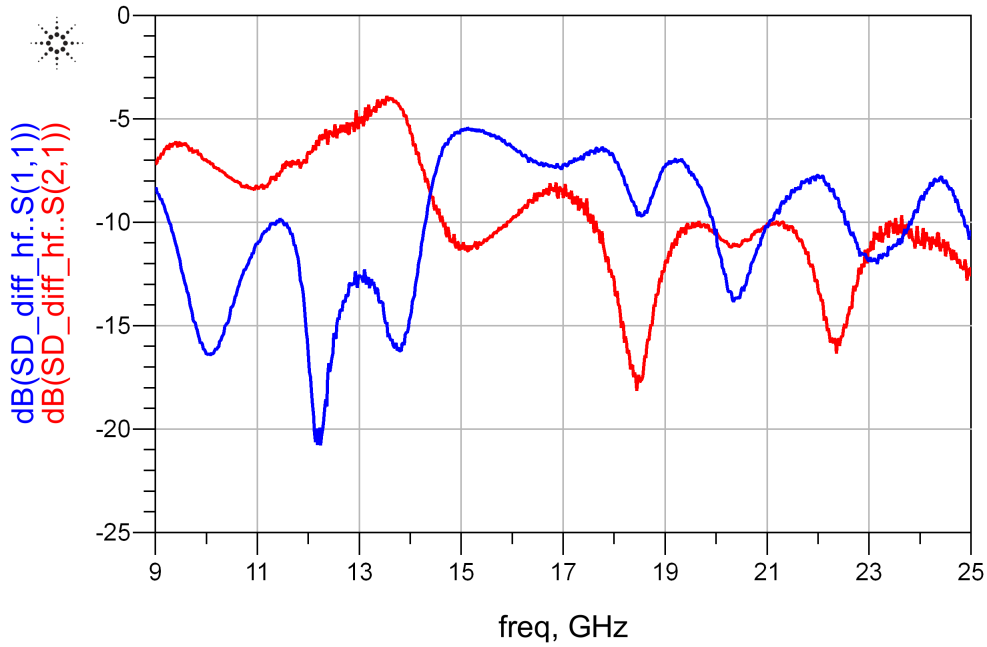

(b) 9 to 25 GHz

Figure 4.7: $|S_{dd11}|$ (blue) and $|S_{dd21}|$ (red) of board SD

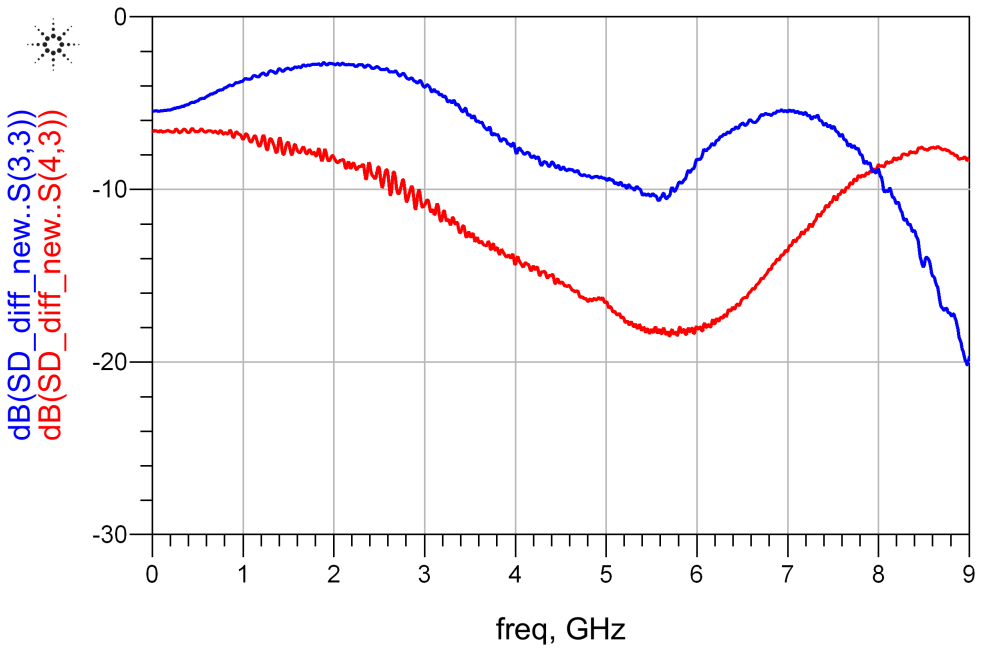

(a) 300 kHz to 9 GHz

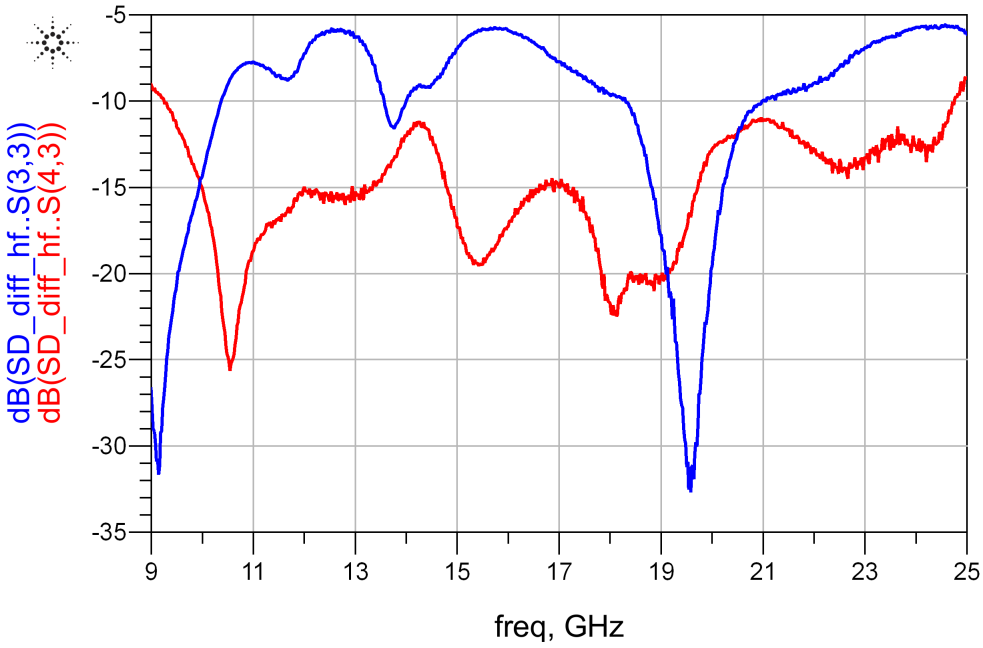

(b) 9 to 25 GHz

Figure 4.8: $|S_{cc11}|$ (blue) and $|S_{cc21}|$ (red) of board SD

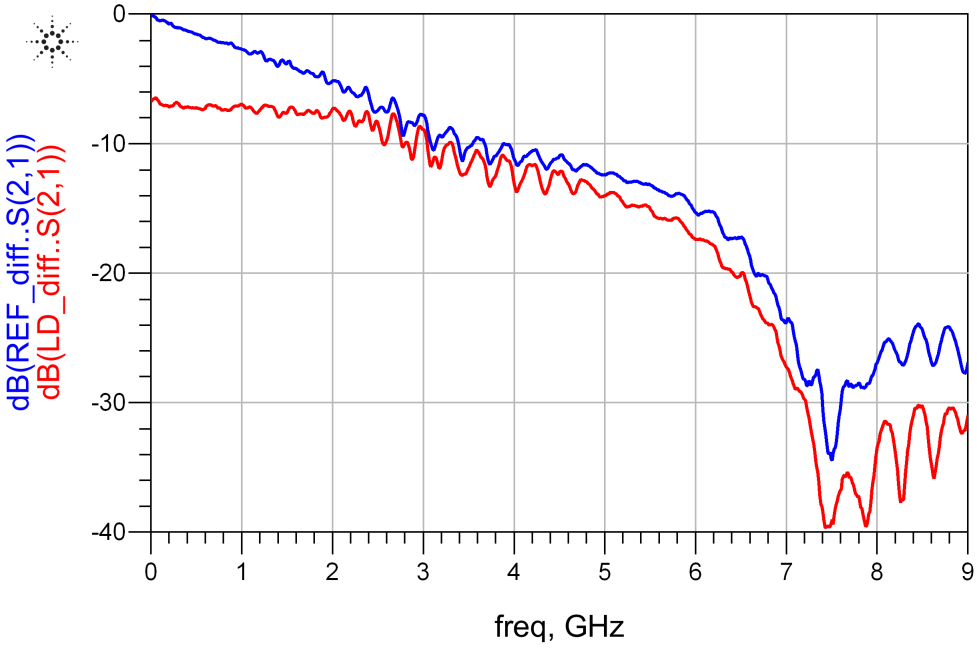

(a) 300 kHz to 9 GHz

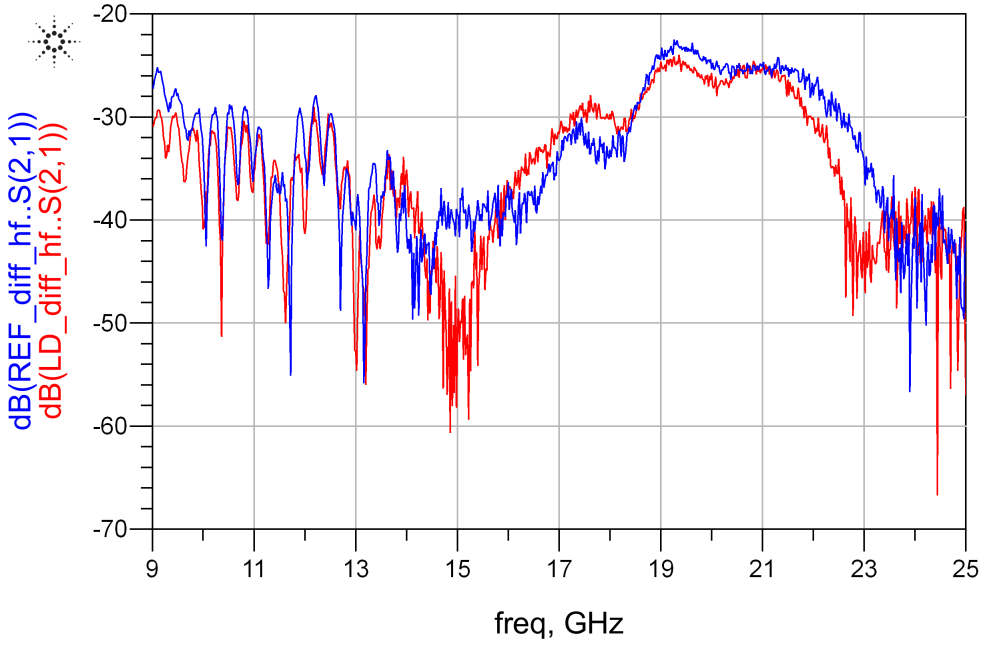

(b) 9 to 25 GHz

Figure 4.9: $|S_{dd21}|$ of boards REF (blue) and LD (red)

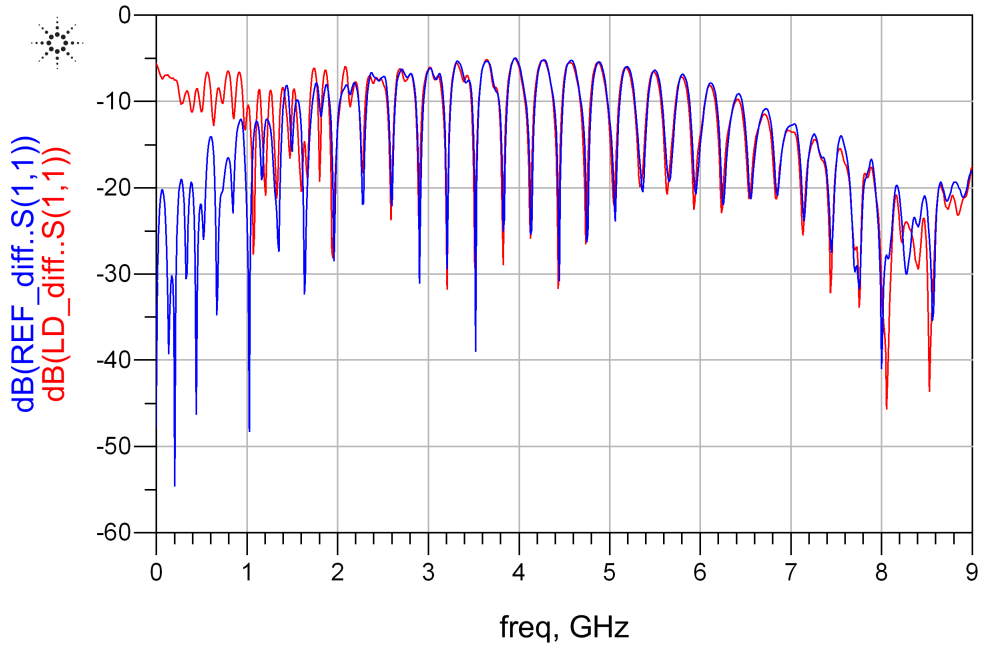

(a) 300 kHz to 9 GHz

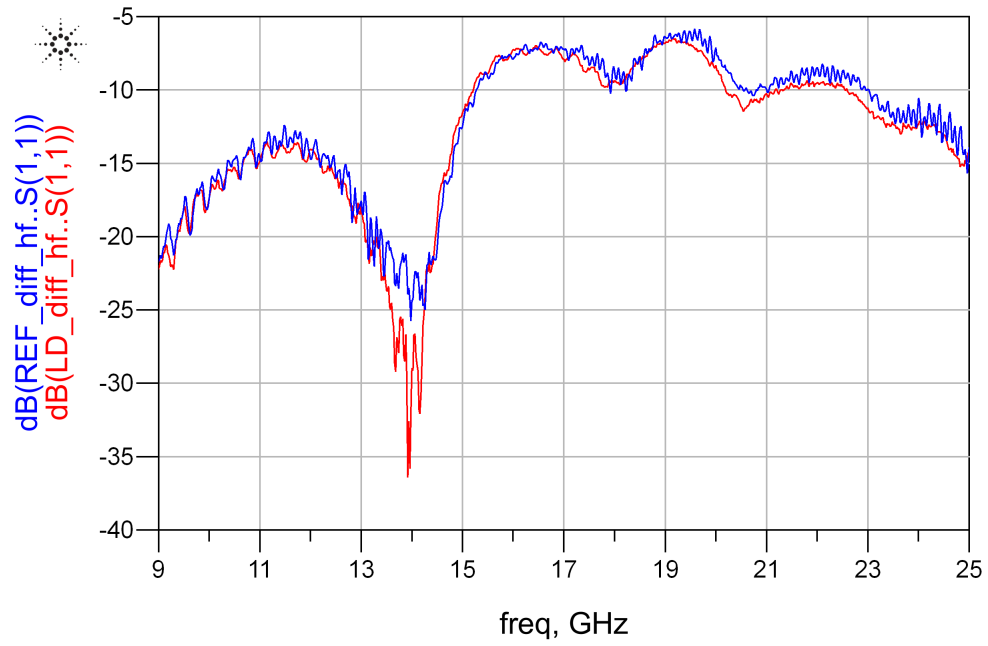

(b) 9 to 25 GHz

Figure 4.10: $|S_{dd11}|$ of boards REF (blue) and LD (red)

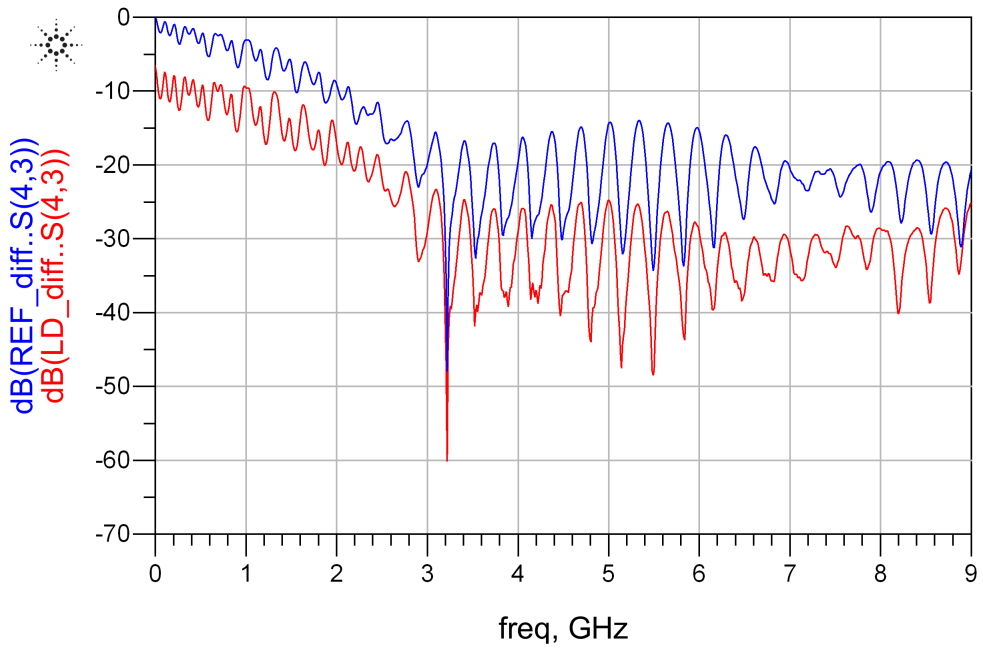

(a) 30 kHz to 9 GHz

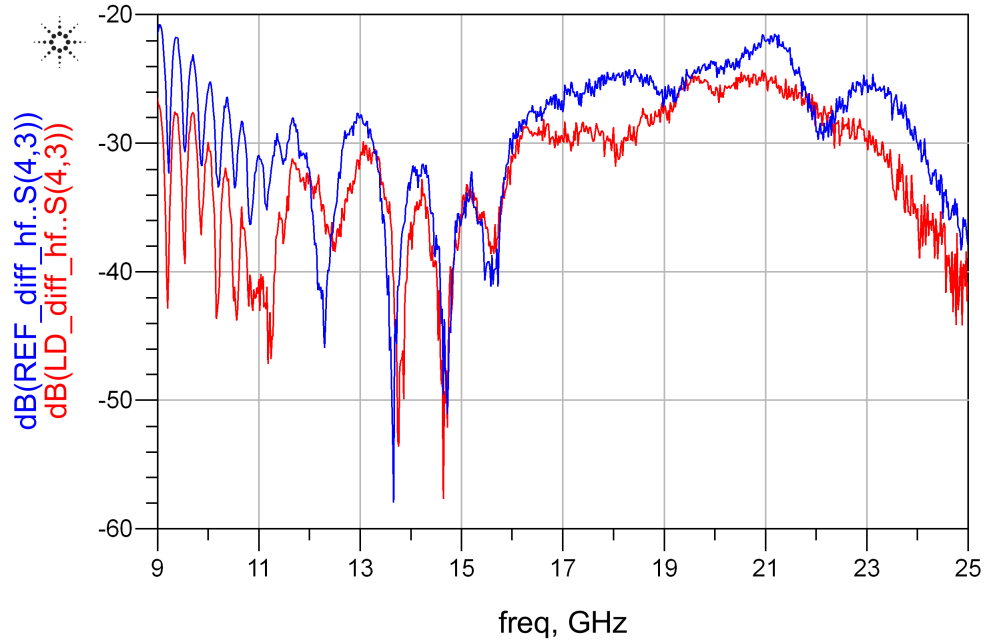

(b) 9 to 25 GHz

Figure 4.11: $|S_{cc21}|$ of boards REF (blue) and LD (red)

Observations

- Figure 4.7 shows the differential insertion loss and input return loss of board SD. $|S_{dd21}|$ shows that the equalizer passes frequencies up to about 7 GHz with minimal loss, while the DC attenuation is roughly 6.7 dB, due to R_T. $|S_{dd11}|$ behaves differently than expected from [1], with minimal return loss in the 3–7 GHz range. This could be due to differences in the manufacturing process, as slightly different substrates were used. At higher frequencies, the behavior is quite varied, with very few regions that might provide decent function, such as at 14 GHz.

- Figure 4.8 shows good CM filtering in the design frequency range, especially at 3–8 GHz, judging by the response of $|S_{cc21}|$. Furthermore, the CM insertion loss is at least 10 dB for essentially the entire range of Figure 4.8b. However, comparing Figures 4.7 and 4.8 reveals that, at frequencies above 9 GHz, there are no common points that display both good equalization and filtering.

- With Figure 4.9, we begin to compare boards LD and REF to see the effects of the DME-CMF when placed after a long channel. Figure 4.9a demonstrates good equalization after a channel, with a clear flattening of $|S_{dd21}|$ up to roughly 3 GHz, as expected from chapter 2. Again we see a DC attenuation of 6.7 dB due to R_T. At higher frequencies, the pattern of behavior of the two boards is very similar, with the LD response tending to be a few dB lower.

- Figure 4.10 again shows very similar behavior between LD and REF, with the main difference being the response up to 1 GHz. Board REF has much lower return loss in this region, yet again due to a lack of the DME-CMF, and therefore any resistors. Additionally, we can see a large dip in $|S_{dd11}|$ at 14 GHz, just as with board SD.

- Figure 4.11 again demonstrates the effectiveness of the DME-CMF in mitigating CM noise. The $|S_{cc21}|$ of LD remains at least 5 dB below that of REF up until about 12 GHz.

4.3.2 Phase Response

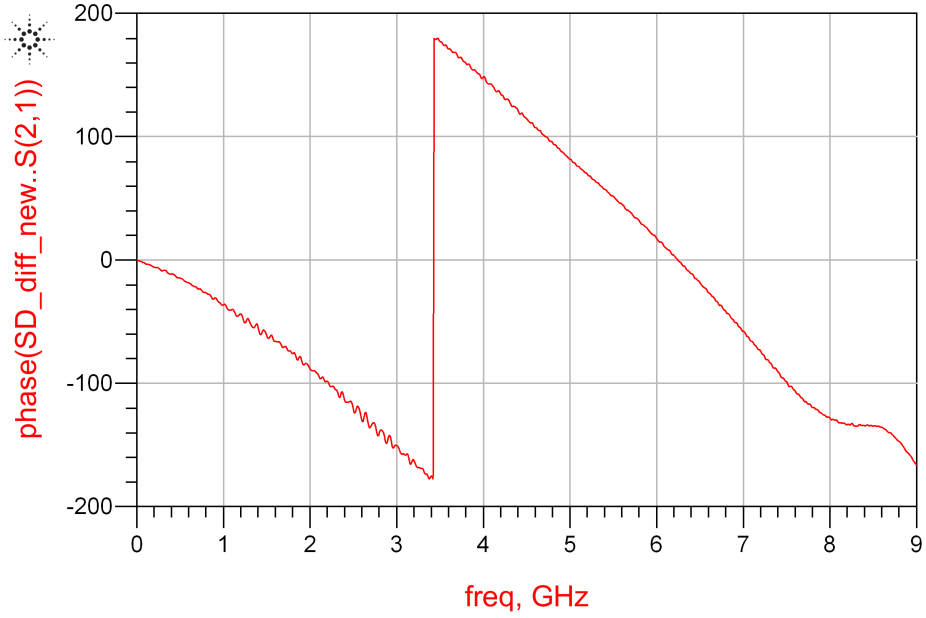

(a) 300 kHz to 9 GHz

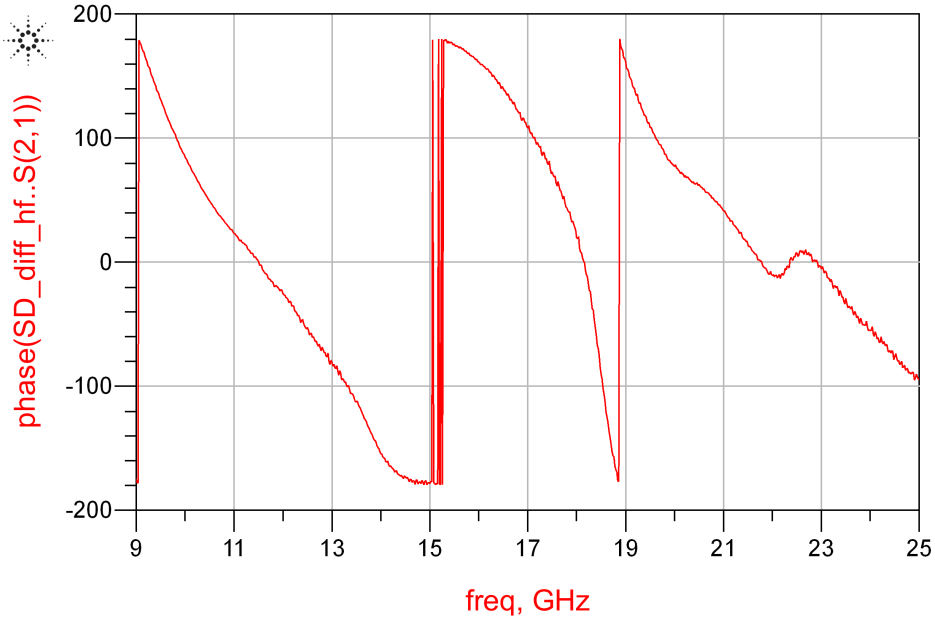

(b) 9 to 25 GHz

Figure 4.12: Phase of S_{dd21} of Board SD

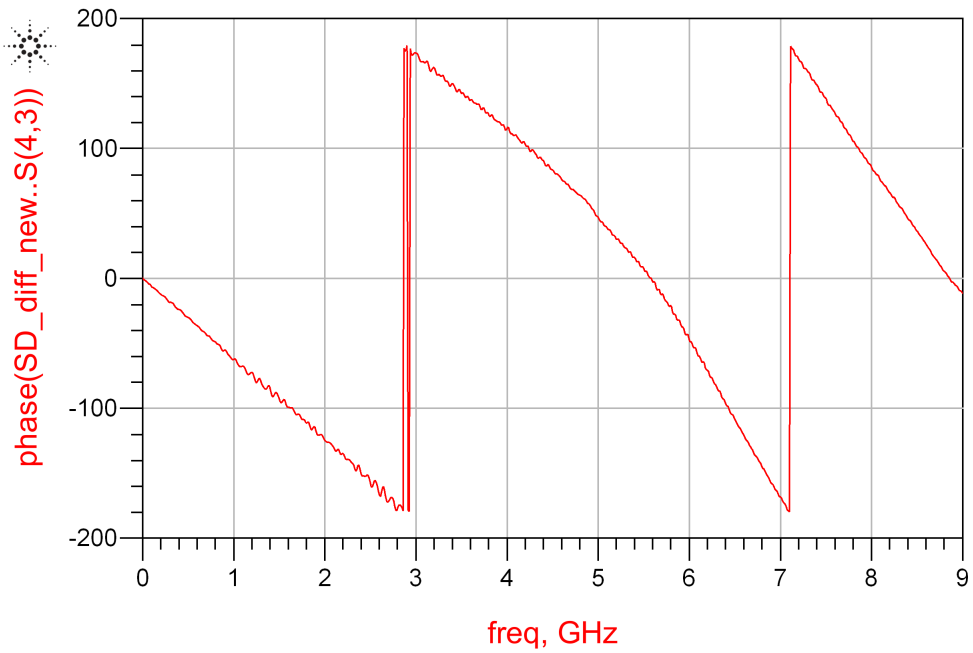

(a) 300 kHz to 9 GHz

(b) 9 to 25 GHz

Figure 4.13: Phase of S_{cc21} of Board SD

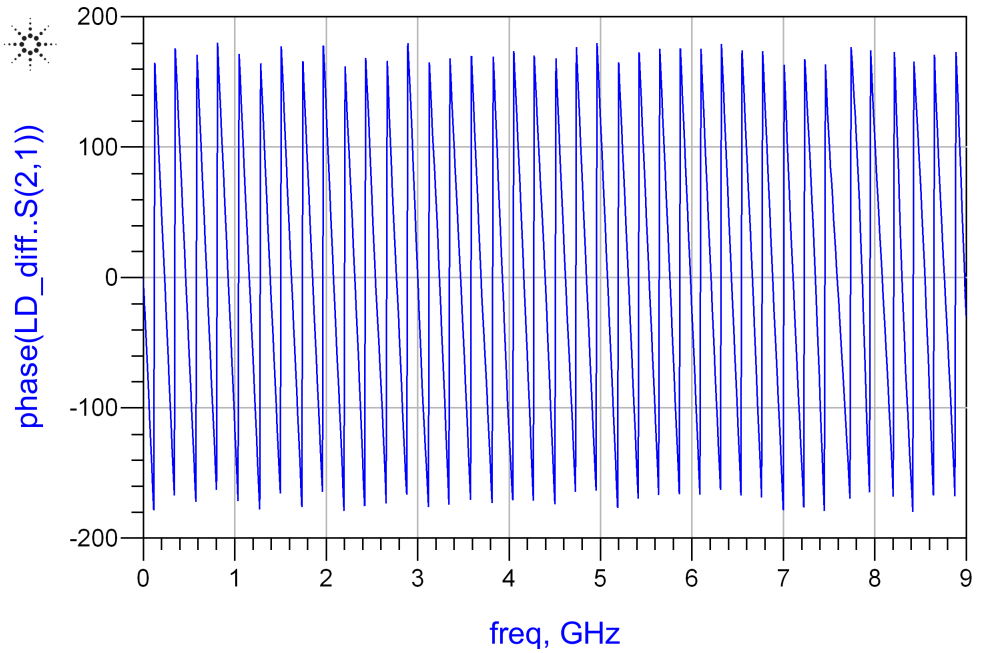

(a) 300 kHz to 9 GHz

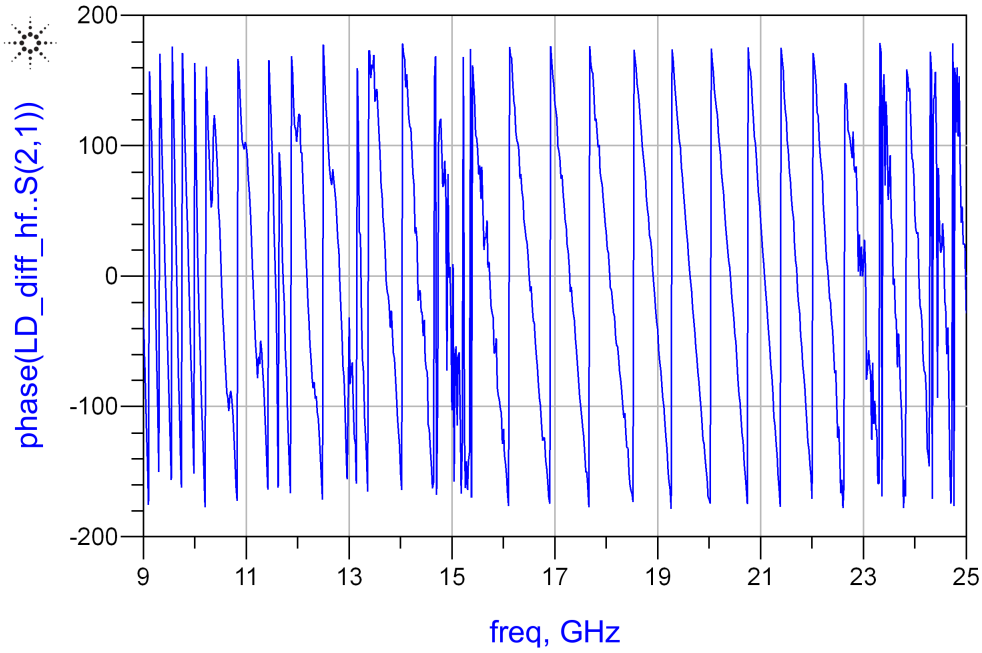

(b) 9 to 25 GHz

Figure 4.14: Phase of S_{dd21} of Board LD

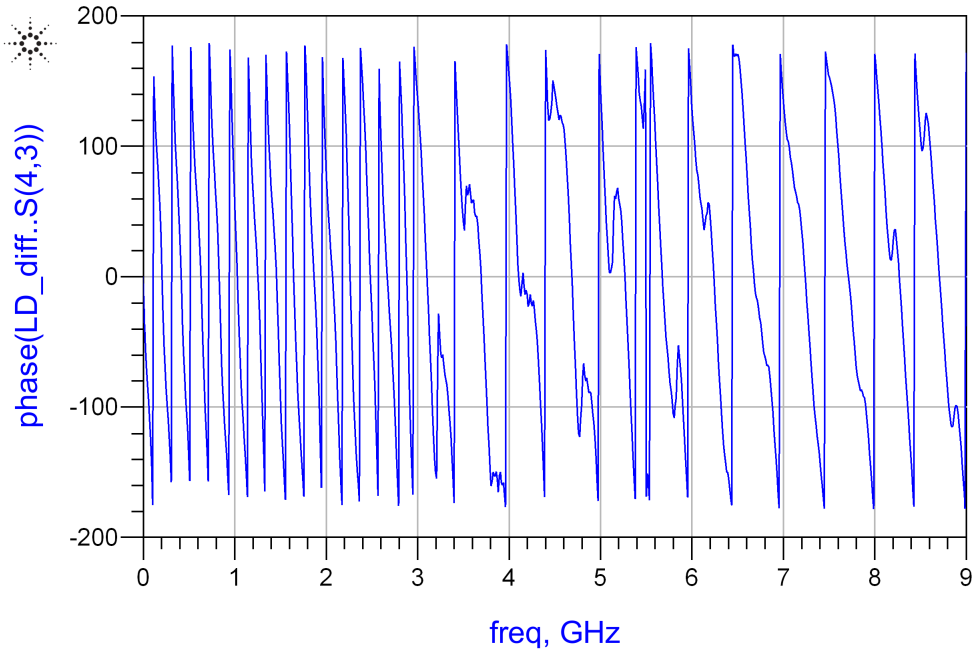

(a) 300 kHz to 9 GHz

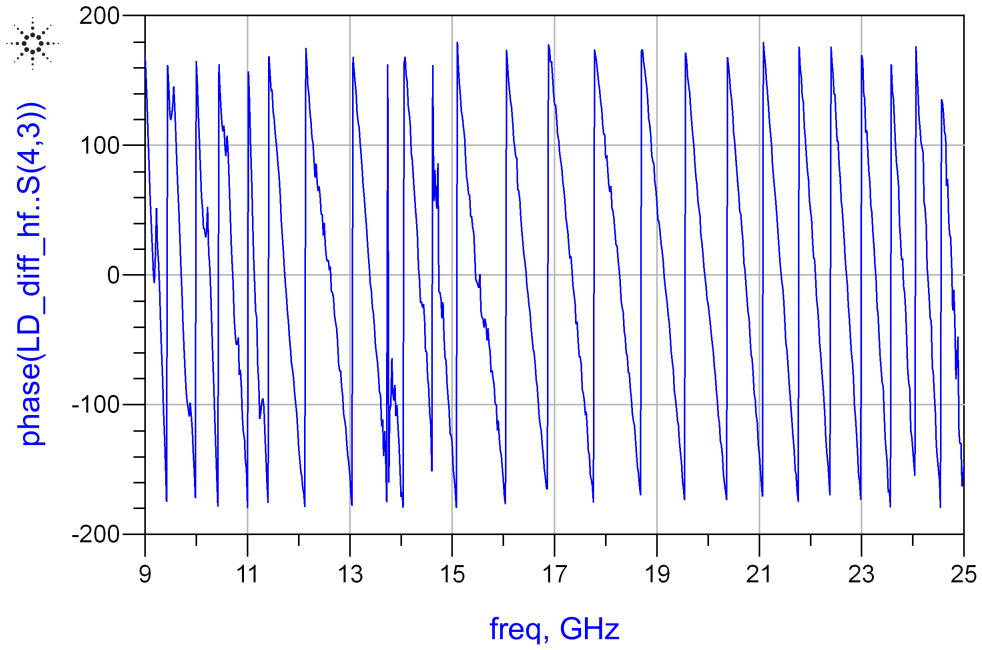

(b) 9 to 25 GHz

Figure 4.15: Phase of $Scc21$ of Board LD

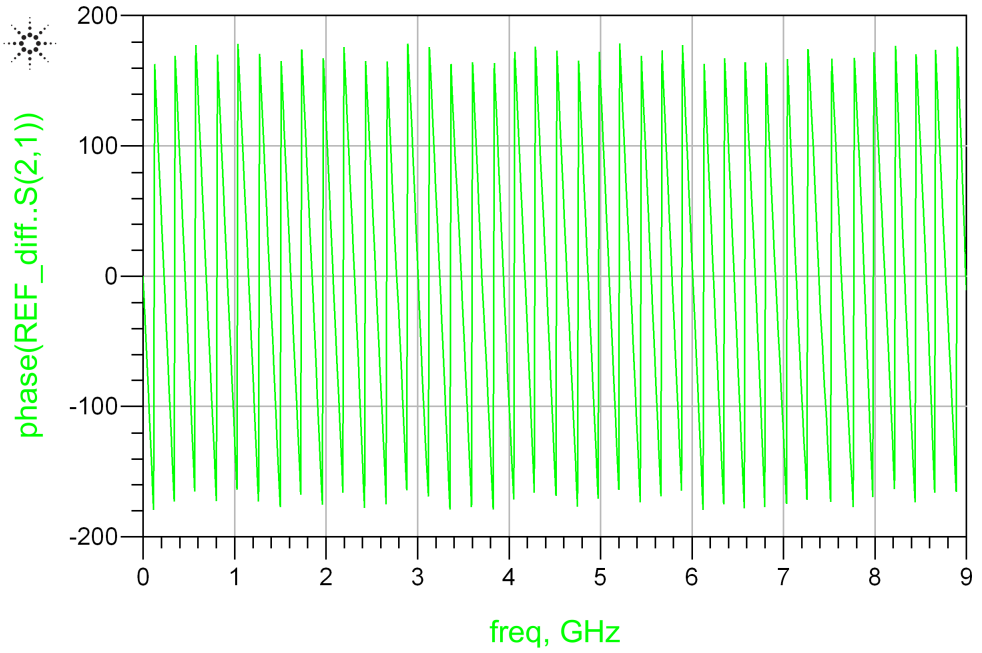

(a) 300 kHz to 9 GHz

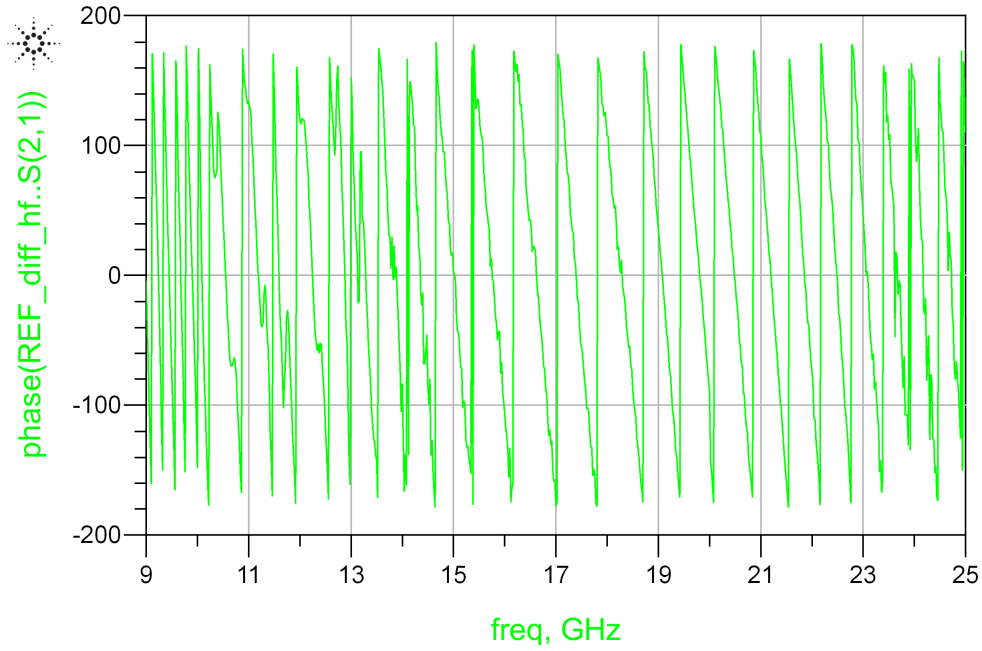

(b) 9 to 25 GHz

Figure 4.16: Phase of S_{dd21} of Board REF

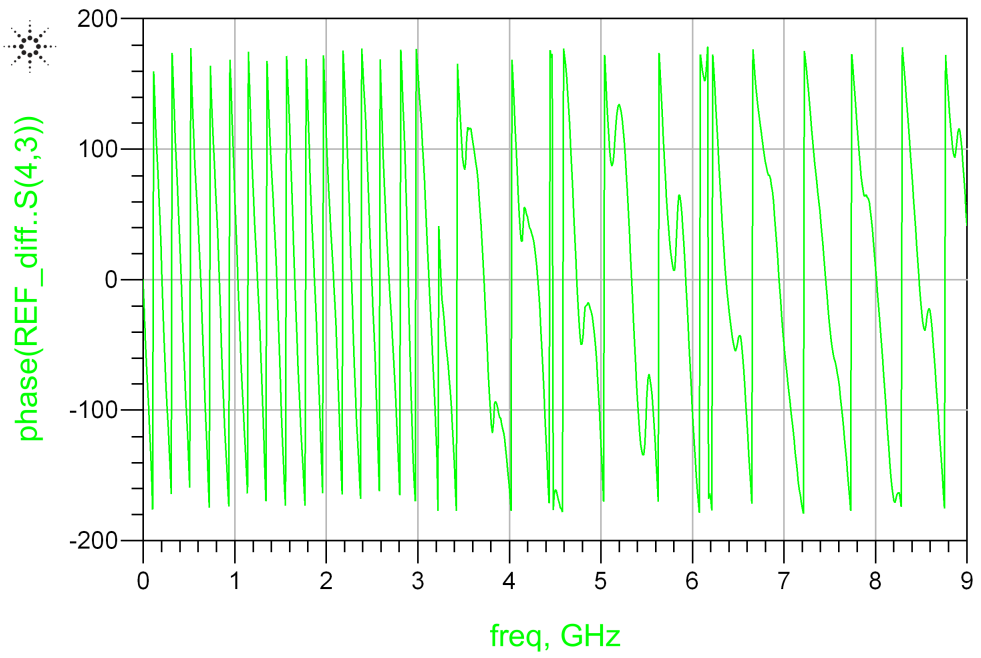

(a) 300 kHz to 9 GHz

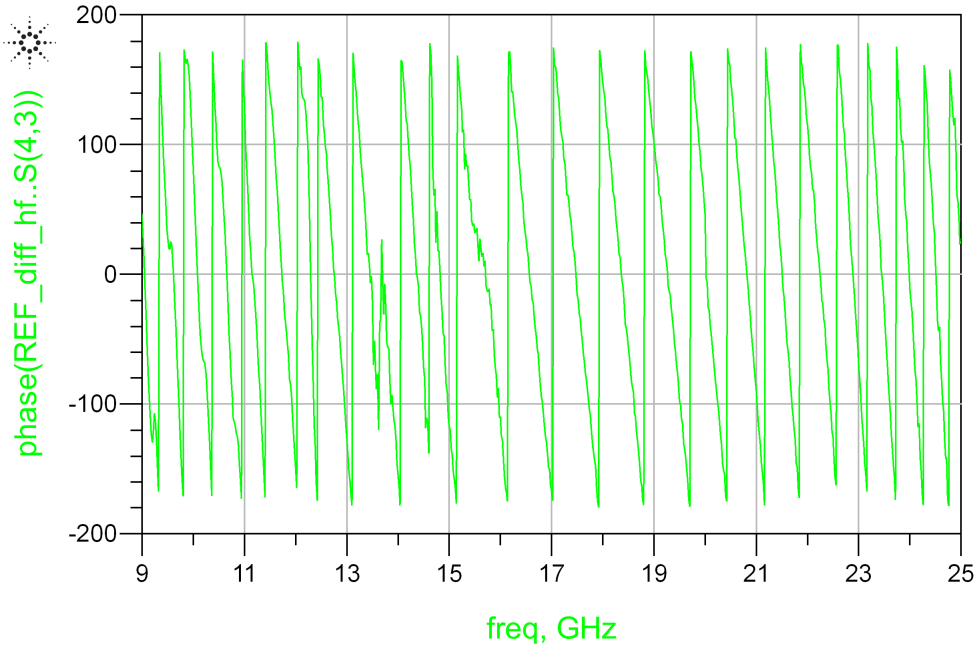

(b) 9 to 25 GHz

Figure 4.17: Phase of S_{cc21} of Board REF

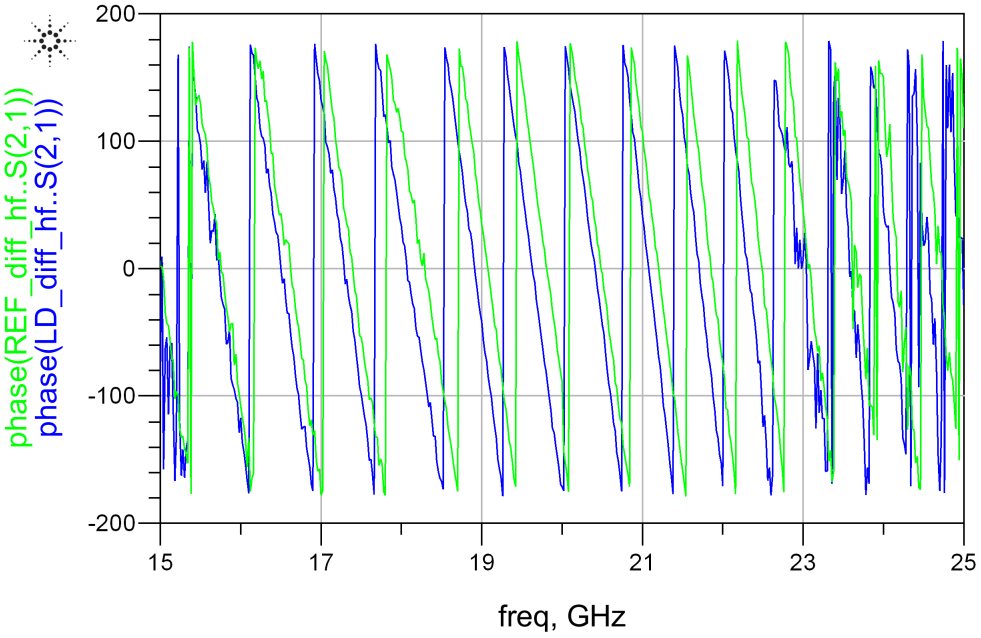

Figure 4.18: Phase of Boards LD (blue) and REF (green) from 15 GHz to 25 GHz

Observations

- Figure 4.12 shows what we would expect to see for the phase of a short channel, remaining mostly linear up to 8 GHz. The DME-CMF does not appear to negatively affect the phase in this region. At 8–15 GHz, slight nonlinearity is seen due to dispersion effects. Above 15 GHz, the effects of dispersion [7] are greater and the phase starts to behave in an aperiodic manner due to higher order modes of propagation.

- Figure 4.13 reveals that the CM phase of board SD seems to be more affected by dispersion, and at lower frequencies, than the DM phase. Again, high frequencies experience additional distortion due to higher order modes.

- The DM phase of board LD seen in Figure 4.14 is as expected for a long channel up to about 10 GHz. At higher frequencies, the effects of higher order modes can be seen.

- Figure 4.15 shows that the CM phase of board LD experiences significant distortion starting as low as 3 GHz. This is most likely due to the impedance discontinuity between the differential channel and the DME-CMF, which constitutes a change in line width and vias through the board.

- Figures 4.16 and 4.17 show that the phase on board REF is very similar to that of board LD, which seems to imply that the phase is mainly determined by the characteristics of the channel, which are identical on both boards.

- Figure 4.18 provides a closer look at the differences between the phase of boards LD and REF at high frequencies. The responses are similar, but the behavior of board REF seems to mirror that of board LD, at a frequency offset of up to 200 MHz. This is again due to dispersion, and not surprising.

4.3.3 Eye Diagrams

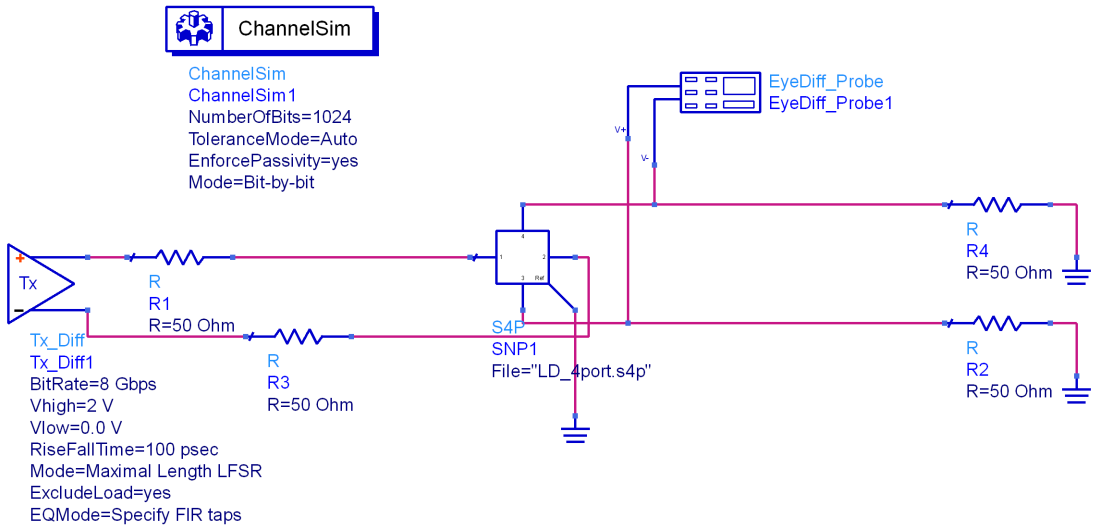

Figure 4.19: Circuit used to simulate eye diagrams in ADS

The circuit in Figure 4.19 was used to generate eye diagrams with a 2^{10} pseudo-random bit sequence of amplitude 2 V. The "S4P" block in the circuit was used to import the S-parameters of the board of interest. Eye diagrams for boards LD and REF were simulated and compared at data rates up to 12 Gb/s, to observe what improvement, if any, is provided by the addition of the DME-CMF. The rise/fall times for the simulations were 100 ps, unless stated otherwise. The eye diagrams follow, succeeded by observations.

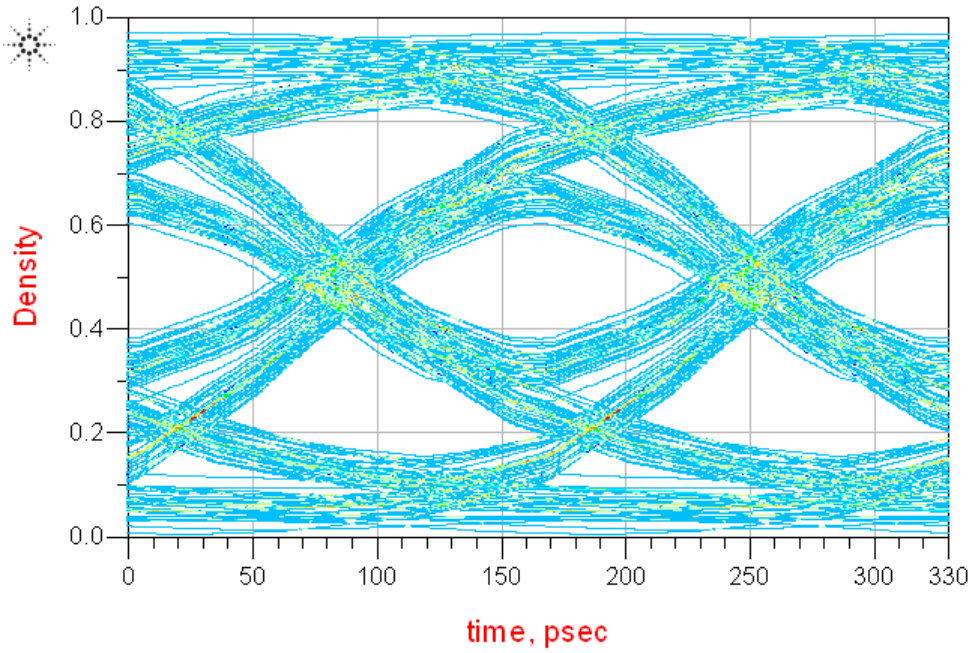

(a) Board REF

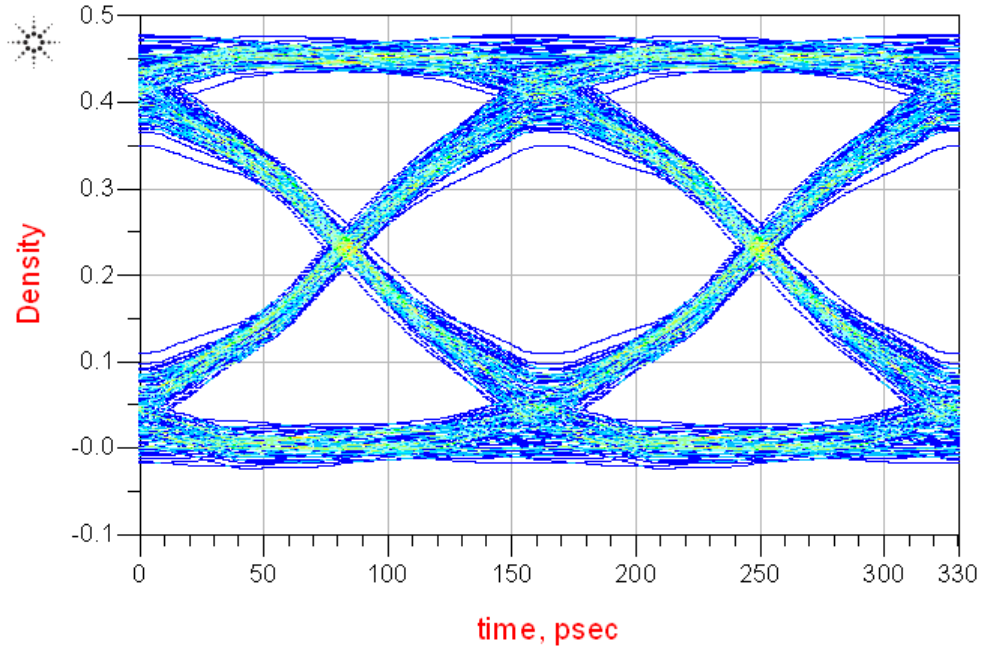

(b) Board LD

Figure 4.20: Eye diagrams at 6 Gb/s

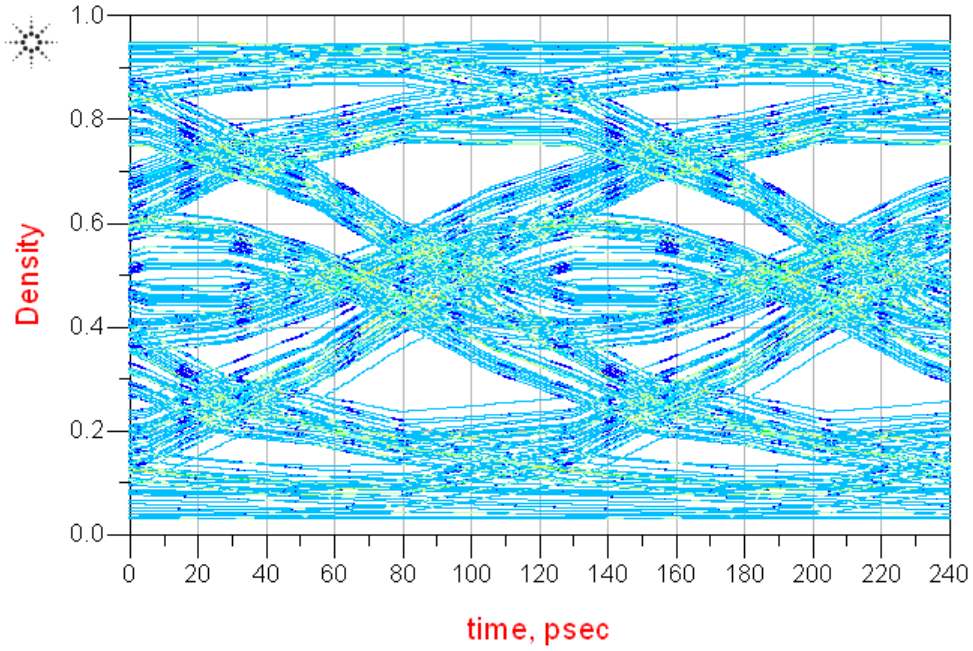

(a) Board REF

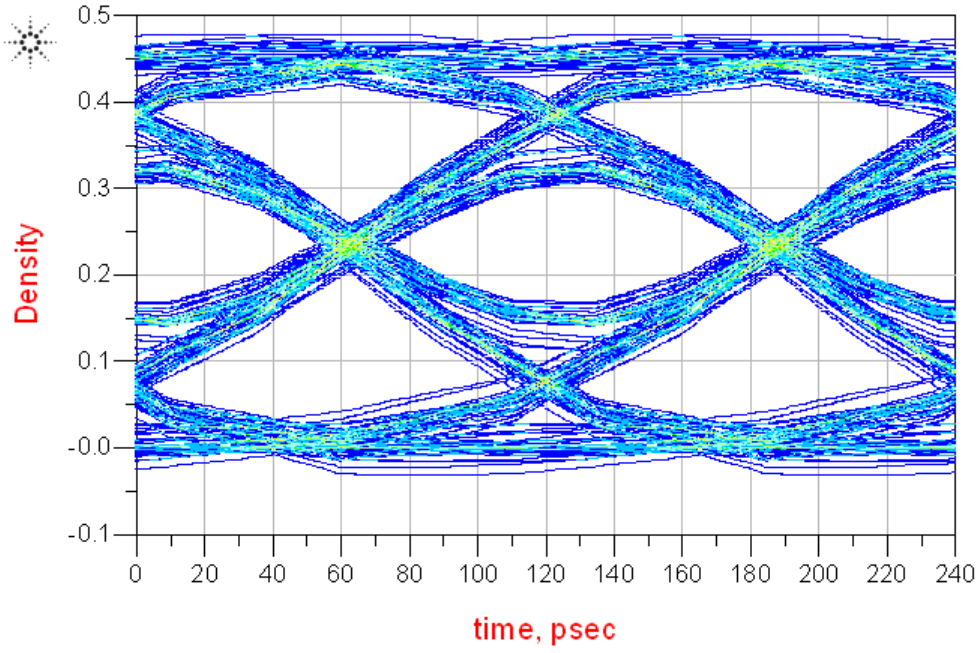

(b) Board LD

Figure 4.21: Eye diagrams at 8 Gb/s

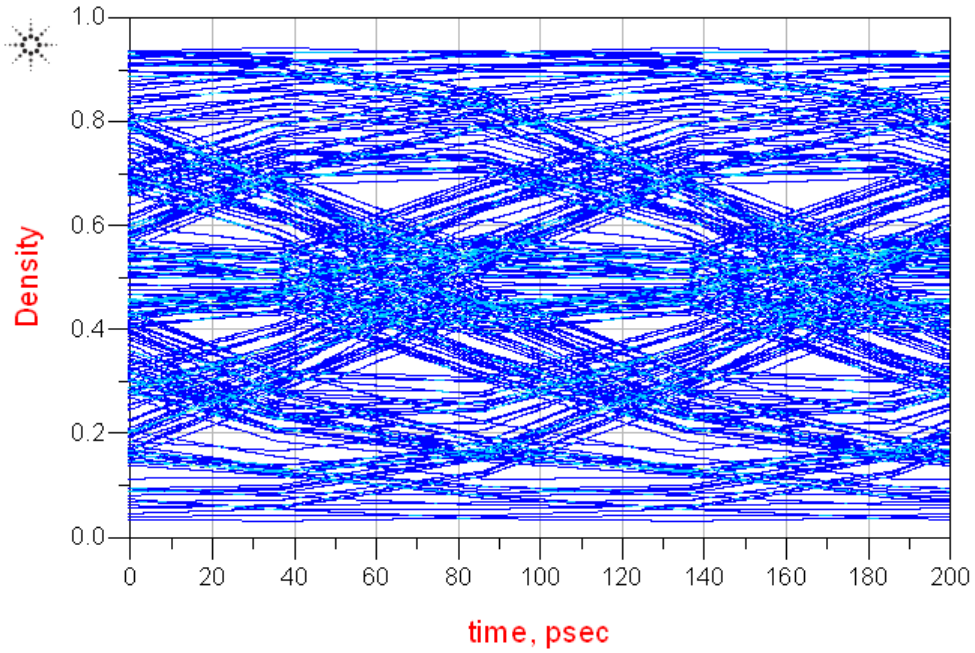

(a) Board REF

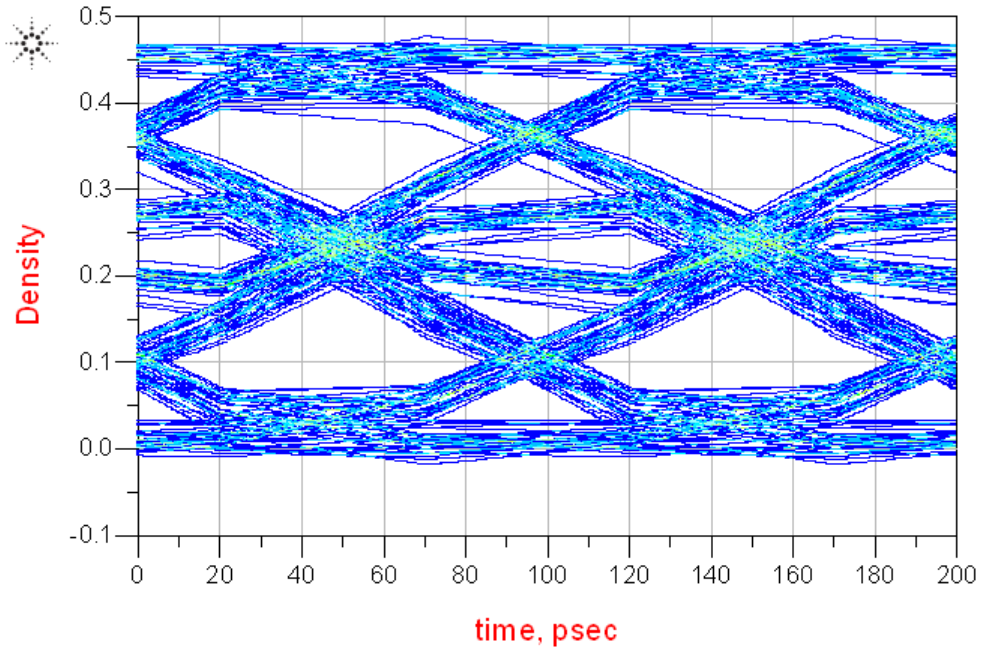

(b) Board LD

Figure 4.22: Eye diagrams at 10 Gb/s

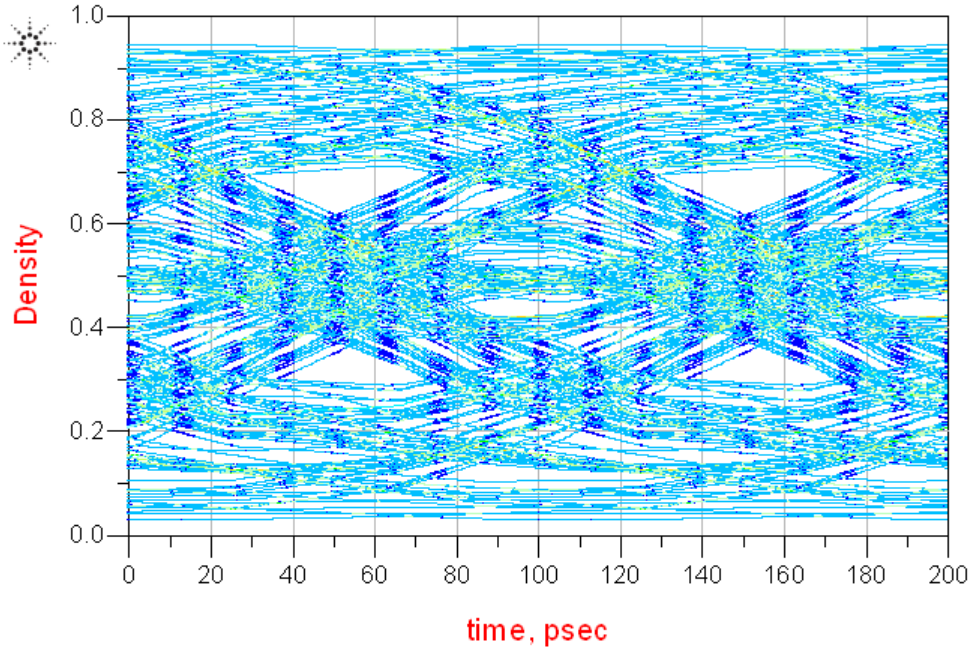

(a) Board REF

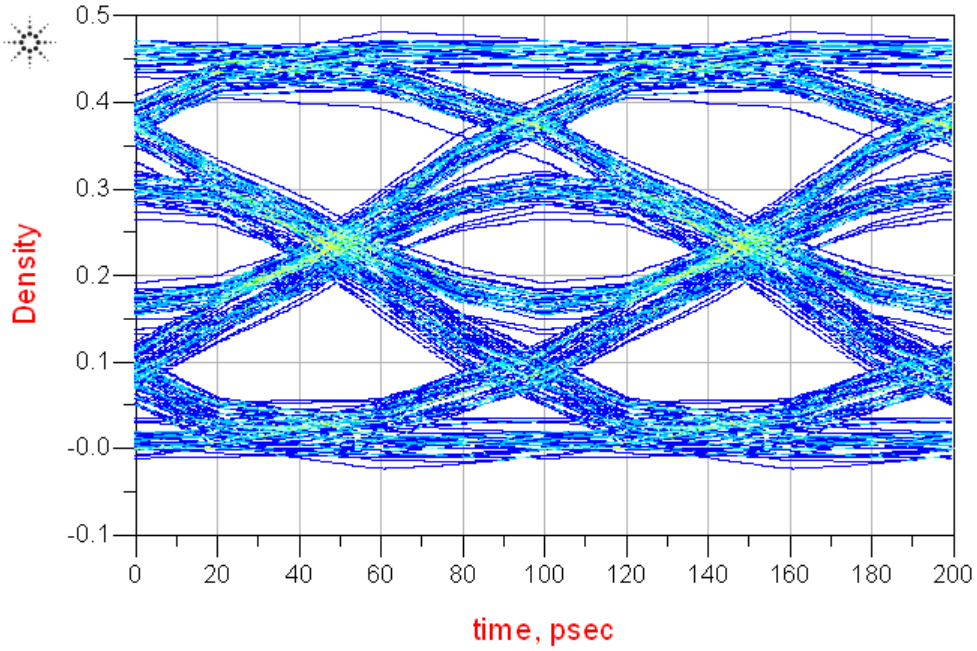

(b) Board LD

Figure 4.23: Eye diagrams at 10 Gb/s with an 80 ps rise/fall time

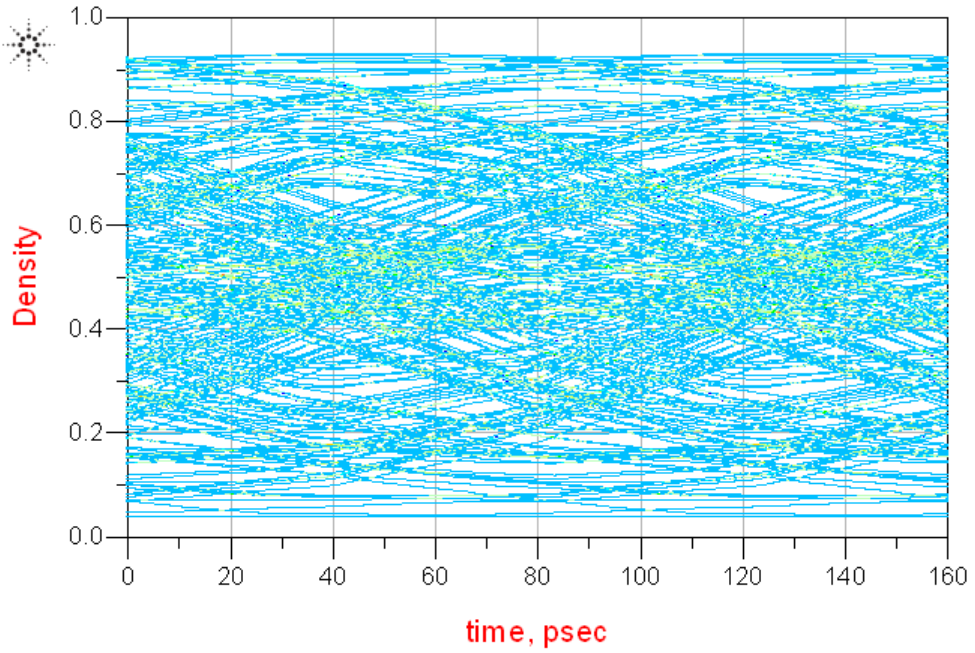

(a) Board REF

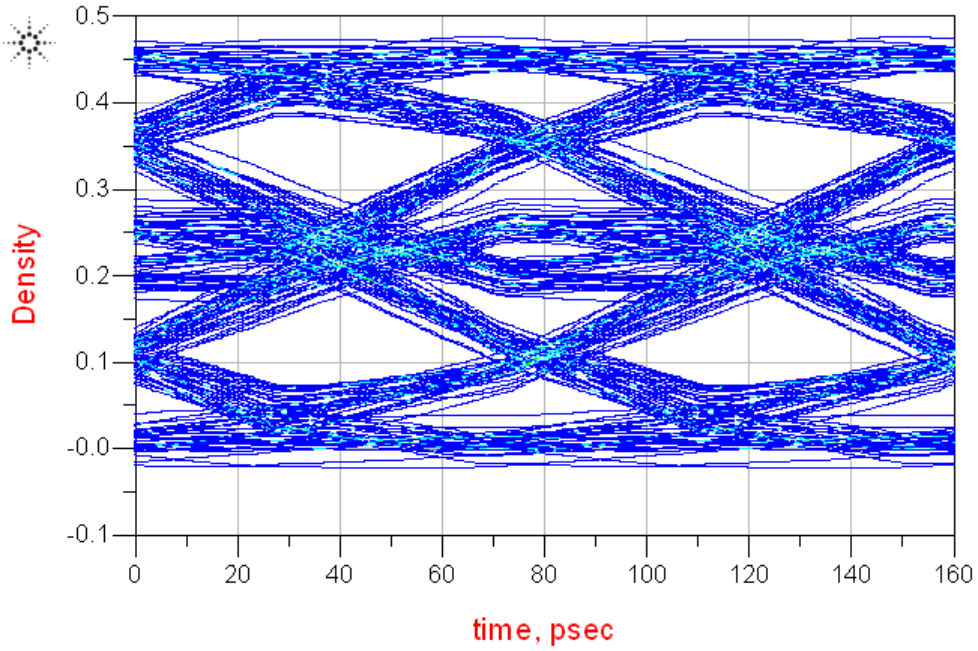

(b) Board LD

Figure 4.24: Eye diagrams at 12 Gb/s with an 80 ps rise/fall time

Observations

- Figure 4.20 shows a simulation of the channel below the target data rate of 8 Gb/s, and while open eyes are observed for both boards REF and LD, there is improvement seen on board LD.

- At the target data rate of 8 Gb/s, Figure 4.21 verifies that while board REF has a closed eye, the addition of the DME-CMF helps to open the eye on board LD. This essentially proves that the DM equalization is functional for data rates up to 8 Gb/s.

- In Figure 4.22, board REF again has a fully closed eye, as is expected for all data rates above 8 Gb/s with no equalization. A very small eye can be observed on board LD, but it is not large enough to claim significant improvement due to the DME-CMF at 10 Gb/s.

- Another simulation was performed at 10 Gb/s, this time with a rise/fall time of 80 ps, and is shown in Figure 4.23. This was done to provide a baseline comparison for simulations at 12 Gb/s, which cannot be done with a 100 ps rise/fall time in Agilent ADS. This simulation shows that with the slightly faster rise/fall time, the eye becomes more open on board LD.

- Figure 4.24 shows that at 12 Gb/s, the improvement due to the DME-CMF is negligible.

CHAPTER 5

CONCLUSION

5.1 Review

The purpose of this thesis was to educate the reader about the DME-CMF and to show that the work done in [1] was reproducible, but also to expand upon that work to see if the design is applicable at higher frequencies and data rates. Chapter 4 showed that the boards designed in [1] (SD, LD, REF) are easily reproduced and function similarly despite some variation in parameters, such as trace length, width, and substrate thickness. The measurement results in section 4.3 clearly show the effectiveness of the differential-mode equalization at and slightly above the intended data rate of 8 Gb/s through observation of eye diagrams. Likewise, the S-parameter magnitude plots confirm a reduction in common-mode noise.

The measurements in chapter 4 also make it clear that the DME-CMF, as currently constructed, cannot function adequately above its targeted frequency and data rate range. Higher order modes of propagation are clearly visible in plots of the phase of all three boards, which would make data sent at equivalent rates irrecoverable. Additionally, the eye diagrams above 8 Gb/s showed minimal or no improvement with the addition of equalization. In fact, increasing functionality up to 25 GHz, as was measured here, may well be impossible with the current microstrip board design. However, with some careful evaluation, a solution that works with slightly higher data rates should be feasible using the current form factor.

5.2 Future Work

The goals of the DME-CMF were to reduce size, cost, and power consumption, and the signal integrity community continues to pursue all three. The researchers behind the original DME-CMF have continued to pursue similar goals, and have experimented with solutions featuring three-layer boards that show promise [9]. On the other side of things, while designers are constantly trying to meet current standards, those standards are constantly being improved upon. The DME-CMF was designed with common interfaces such as USB 3.0 and PCI Express 3.0 in mind, but as these advance, so too must the goals of the designers. Interest has also been expressed in using this technology to perform equalization and filtering after the main channel in Serializer/Deserializer (SerDes) applications.

APPENDIX A

S-PARAMETER CONVERSION

The following MATLAB code will convert 4-port S-parameter data in .s4p format to differential-mode S-parameters in .s2p format:

```
S_4port = sparameters('REF_4port_hf.s4p');
disp(S_4port)
params = S_4port.Parameters;
freq = S_4port.Frequencies;

M = (1/sqrt(2))*[1,-1,0,0;0,0,1,-1;1,1,0,0;0,0,1,1];
M_inv = inv(M);

for i = 1:801
    diff_S(:,:,i) = M*params(:,:,i)*M_inv;
end

S_diff = sparameters(diff_S,freq);
rfwrite(S_diff,'REF_diff_hf.s2p');
```

REFERENCES

[1] C.-K. Cheng, Y.-J. Cheng , H.-H. Chuang and T.-L. Wu, "Novel differential-mode equalizer with broadband common-mode filtering for Gb/s differential-signal transmission," *IEEE Trans. Compon. Packag. Manufact. Technol.*, vol. 3, no. 9, pp. 1578–1587, 2013.

[2] Y. Shim, W. Lee, E. Song, J. Cho, and J. Kim, "A compact and wide-band passive equalizer design using a stub with defected ground structure for high speed data transmission," *Microwave and Wireless Components Letters, IEEE*, vol. 20, no. 5, pp. 256–258, 2010.

[3] C.-H. Tsai and T.-L. Wu, "A broadband and miniaturized common-mode filter for gigahertz differential signals based on negative-permittivity metamaterials," *Microwave Theory and Techniques, IEEE Transactions on*, vol. 58, no. 1, pp. 195–202, 2010.

[4] S.J. Franke, *ECE 453 Wireless Communications Systems Course Notes, Fall 2013.* Self-published, 2013, Course notes for ECE 453, University of Illinois.

[5] Maxim Integrated Products, *Single-Ended and Differential S-Parameters*, 2008, Appl. Note HFAN.5.1.0.

[6] Agilent Technologies, *Eye Diagram Measurements in Advanced Design System*, 2008, Note 5989-9453EN.

[7] H. Cory, "Dispersion characteristics of microstrip lines," *Microwave Theory and Techniques, IEEE Transactions on*, vol. 29, no. 1, pp. 59–61, 1981.

[8] J. P. Dunsmore, *Handbook of Microwave Component Measurements.* Wiley, 2012.

[9] C.-Y. Hsiao and T.-L. Wu, "A novel dual-function circuit combining high-speed differential equalizer and common-mode filter with an additional zero," *Microwave and Wireless Components Letters, IEEE*, vol. 24, no. 9, pp. 617–619, 2014.